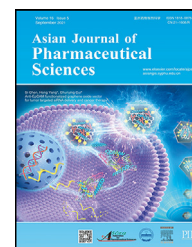


Available online at www.sciencedirect.com

ScienceDirect

journal homepage: www.elsevier.com/locate/AJPS

Original Research Paper

Dual pH and microbial-sensitive galactosylated polymeric nanocargoes for multi-level targeting to combat ulcerative colitis

Mahira Zeeshan^{a,b,e}, Qurat Ul Ain^a, Benno Weigmann^b, Darren Story^{c,d}, Bryan R. Smith^{c,d}, Hussain Ali^{a,*}

^aDepartment of Pharmacy, Faculty of Biological Sciences, Quaid-i-Azam University, Islamabad 45320, Pakistan

^bDepartment of Medicine 1, University of Erlangen-Nuremberg, Kussmaul Campus for Medical Research, Erlangen 91052, Germany

^cBiomedical Engineering Department, Michigan State University, East Lansing 48824, USA

^dInstitute for Quantitative Health Science and Engineering, Michigan State University, East Lansing 48824, USA

^eFaculty of Pharmacy, Capital University of Science and Technology, Islamabad 44000, Pakistan

ARTICLE INFO

Article history:

Received 15 February 2023

Revised 15 May 2023

Accepted 6 June 2023

Available online 26 July 2023

Keywords:

Galactosylated nanocargoes

pH-sensitive drug delivery

Pullulan

Microbial sensitive

Ulcerative colitis

Macrophage galactose type-lectin C

ABSTRACT

Ulcerative colitis (UC) is a type of inflammatory bowel disease characterized by inflammation, ulcers and irritation of the mucosal lining. Oral drug delivery in UC encounters challenges because of multifaceted barriers. Dexamethasone-loaded galactosylated-PLGA/Eudragit S100/pullulan nanocargoes (Dexa-GP/ES/Pu NCs) have been developed with a dual stimuli-sensitive coating responsive to both colonic pH and microbiota, and an underneath galactosylated-PLGA core (GP). The galactose ligand of the GP preferentially binds to the macrophage galactose type-lectin-C (MGL-2) surface receptor. Therefore, both stimuli and ligand-mediated targeting facilitate nanocargoes to deliver Dexa specifically to the colon with enhanced macrophage uptake. Modified emulsion method coupled with a solvent evaporation coating technique was employed to prepare Dexa-GP/ES/Pu NCs. The nanocargoes were tested using *in vitro*, *ex vivo* techniques and dextran sodium sulfate (DSS) induced UC model. Prepared nanocargoes had desired physicochemical properties, drug release, cell uptake and cellular viability. Investigations using a DSS-colitis model showed high localization and mitigation of colitis with downregulation of NF- κ B and COX-2, and restoration of clinical, histopathological, biochemical indices, antioxidant balance, microbial alterations, FTIR spectra, and epithelial junctions' integrity. Thus, Dexa-GP/ES/Pu NCs found to be biocompatible nanocargoes capable of delivering drugs to the inflamed colon with unique targeting properties for prolonged duration.

© 2023 Shenyang Pharmaceutical University.

This is an open access article under the CC BY-NC-ND license

(<http://creativecommons.org/licenses/by-nc-nd/4.0/>)

* Corresponding author.

E-mail address: h.ali@qau.edu.pk (H. Ali).

Peer review under responsibility of Shenyang Pharmaceutical University.

<https://doi.org/10.1016/j.ajps.2023.100831>

1818-0876/© 2023 Shenyang Pharmaceutical University. This is an open access article under the CC BY-NC-ND license

(<http://creativecommons.org/licenses/by-nc-nd/4.0/>)

1. Introduction

Ulcerative colitis (UC) is the most prevalent form of inflammatory bowel disease (IBD) affecting the mucosal lining of the colon and rectum. The main pathophysiological features are innate immune system imbalance and impaired mucosal healing [1]. The immune disturbance generates a series of events that recruit immune cells to inflamed regions. Initially, recruited macrophages acquired the M1 phenotype to mediate host defense actions and produce excessive pro-inflammatory cytokines and oxygen radicals that exacerbate inflammation. The macrophages have overexpressed surface receptors to mediate immune hemostasis [2]. These receptors have recently gained attention for their potential for drug delivery [2].

Several therapeutic options are available for managing UC including aminosalicylates, corticosteroids, immunosuppressants and biologics. However, drugs display pharmacokinetic limitations, adverse effects, drug resistance, a higher cost, and low patient compliance, limiting their therapeutic success [3,4]. Oral delivery of therapeutic agents being the most convenient and direct route to the inflamed gastrointestinal tract (GIT) faces multiple pathophysiological barriers like degradation by the gastric pH, GI enzymes or biliary fluid, first pass effect, and rapid clearance due to heavy diarrhea inherent to UC, making such therapeutic strategies less efficient in crossing the mucus layer [3]. Scientific advancements in nanomedicine offer better and safer options for targeting the inflamed intestine [4]. Various tailor-made nanoparticles provide a better solution for site-specific colon drug delivery. For instance, stimuli-sensitive nanoparticles and particularly pH-sensitive nanoparticles, have gained wide attention based on their success in murine models [5–8]. Most relevantly, Eudragit S100 (ES) based polymers are employed for colon targeting, given their pH responsive nature enabling disintegration and drug release only at a specific pH [7–9]. To offer more precise colon targeting during inflammation, the nanoparticles sensitive to inflammation specific conditions like reactive oxygen species [10,11] were developed to target the colon inflammatory region. The combination of sustained release polymers like PLGA, chitosan, etc. with pH-sensitive polymers enabled long-term IBD therapy [7,8]. Moreover, researchers used natural carbohydrate polymers degradable by colonic resident bacteria for nanoparticle drug delivery to the colon [12,13]. In this quest, pullulan is a neutral polysaccharide with widespread biomedical applications given its biodegradability, adhesiveness, film-forming nature and mechanical strength. Besides, it can be used as a probiotic, binder, stabilizer and emulsifier, and is susceptible to degradation by the pullulanase enzyme in colonic bacteria [14,15]. Recently, pullulan was employed for colon targeting purposes with good *in vitro* outcomes [16,17]. However, pullulan-based nano-formulations have not yet been explored in animal models of IBD.

Since there are inter- and intra-animal differences in colon pH and natural flora, translating the pH-sensitive or microbial responsive concept into humans necessitates additional research [3]. In the search for better therapy, the second generation of ligand bound nanocarriers have been developed

that target with greater binding affinity to the specific intestinal immune cell or colon cell membrane receptor (e.g., CD71, CD301b/macrophage galactose type C-type lectin 2 (MGL2), folate, transferrin, or mannose receptors) [18–21]. However, it is not clear that ligand-anchored nanocarriers can survive the harsh conditions of the GIT and reach the colon without any dose dumping.

We hypothesized to develop nanocargoes with a dual stimuli-sensitive coat (pH-sensitive & microbial-sensitive polysaccharide) around a glycol-ligand anchored core for specific drug delivery to the inflamed colon. Based on GIT pathophysiological differences and macrophage receptor overexpression, the nanocargoes would be able to achieve organ- and tissue-level specificity by exploiting the colon microenvironment and macrophage ligand potential.

Here, the microbial sensitivity of pullulan and pH sensitivity of Eudragit S100 (ES100) were used to envelop the inner D-galactose conjugated PLGA core (GP) to form a smart, dual stimuli-sensitive, biofunctionalized ES100/Pullulan coated D-galactose-PLGA nanocargoes (GP/ES/Pu NCs). The ES outer layer is responsive to a pH threshold of 7, corresponding to colon pH [3]; and pullulan is a probiotic, degradable by pullulanase produced by colon microbes [22]. The combination of the two polymers imparts dual stimuli-sensitive (pH and microbial) properties to the nanocargoes that enable colon specific targeting and overcome inter- and intra-individual variations in GI conditions [23]. In the colon, the stimuli sensitive coat dissolves exposing the GP core, thus allowing the GP-galactose ligand to target intestinal macrophages via MGL-2 receptors and overcome physiological barriers [3,24]. The corticosteroid dexamethasone (Dexa) was chosen as a prototype drug to be loaded into the nanocargoes to enhance the therapeutic action in UC. Dexa, when released inside the cells, binds to the cytoplasmic glucocorticoid receptors (GR) causing them to migrate to the nuclear domain where GR interacts with various pathways, including NF- κ B and COX-2 inhibition, retarding pro-inflammatory cytokines and signaling [25,26]. Therefore, the novel Dexa loaded GP/ES/Pu NCs (Dexa-GP/ES/Pu NCs) can cross the pathophysiological barriers both at organ and tissue levels across the GIT in colon inflammation.

For this project, we prepared and optimized the GP polymer as described in our previous work [27]. Then Dexa-GP/ES/Pu NCs were developed using the modified emulsion method and coating evaporation techniques. After physicochemical characterization, *in vitro* drug release, cell-based biocompatibility, and uptake studies were performed. The *in vivo* targeting potential and therapeutic efficacy of Dexa-GP/ES/Pu NCs were tested in the dextran sodium sulfate (DSS) induced UC mouse model. Additionally, toxicology in healthy mice was studied to assess Dexa-GP/ES/Pu NCs biocompatibility within living bodies.

2. Material and methods

2.1. Materials

PLGA (Resomer® 502, 50:50, MW 7,000–17,000) and ES100 (1:2) were obtained from Evonik Industries (Darmstadt,

Germany). Pullulan (CAS: 9057-02-7, MW 500–700 kDa) was gifted from Xi'an Sgonek Biological Technology Co., Ltd (China). Dexa (MW 392.46), polyvinyl alcohol (PVA; Mowiol[®], MW 31,000), D-galactose (MW 180.68), DSS (MW 40,000), organic solvents, Evans blue had been taken from Sigma Aldrich (Germany). HCl, potassium dihydrogen phosphate (KH₂PO₄), and disodium hydrogen phosphate (Na₂HPO₄·2H₂O) were purchased from BDH Laboratory Supplies (Poole, UK). Cetyltrimethylammonium bromide (CTAB), rhodamine-B, thioglycolate, GSH, GST, catalase, thiobarbituric acid, 3-(4,5-dimethylthiazol-2-yl)-2,5-diphenyltetrazolium bromide (MTT), cRPMI-1640, fetal bovine serum (FBS), penicillin/ streptomycin, methane sulfonic acid, and N, N-dimethylformamide (DMF) were purchased from Millipore Sigma Aldrich (St Louis, MO, USA). Propidium iodide (PI) and annexin-V from BD Biosciences (San Diego, CA, USA)

2.2. Animals for the disease model

Male BALB/c mice, 3–4 weeks old, were purchased from NIH, Islamabad, and kept under protocols prescribed for the care and use of laboratory animals under QAU, Islamabad bioethical committee, and NIH. The protocol for animal studies of the project was approved under protocol no. BEC-FBS-QAU2020–238. All experiments were designed to comply with ARRIVE guidelines. Ulcerative colitis was developed in the mice through the administration of 3% (w/v) DSS in the drinking water for 7 d. Mice were observed daily for the development of colitis through clinical symptoms like decline in body weight, rectal bleeding, diarrhea, and signs of distress, as already reported [28].

2.3. Synthesis of polymer and characterization

PLGA derived polymer containing D-galactose residue (GP) was synthesized by reacting D-galactose and PLGA (50:50) under vacuum conditions. The procedure and reaction conditions were optimized in our previous study [27]. The derived polymer was confirmed through FTIR and NMR characterization techniques.

2.4. Preparation of Dexa-GP/ES NPs, Dexa-GP/Pu NPs and Dexa-GP/ES/Pu NCs

Dexa-GP/ES NPs were prepared by dissolving Dexa (1 mg) and GP (10 mg) in ethyl acetate and adding the organic solution into an aqueous phase containing ES100, 2% PVA, methanol, and 0.1 N NaOH in a dropwise manner, followed by strenuous sonication using a probe sonicator (20 kHz, Misonix- XL-2000 series) for about 1 min and kept stirred for 2–4 h. The ratio of the organic-aqueous phase was kept at 1:4 after some preliminary experiments. Stirring was continued overnight for the evaporation of organic solvents. For Dexa-GP/Pu NPs, the aqueous phase was replaced with pullulan (20 mg) and 2% PVA only.

Dexa-GP/ES/Pu NCs were fabricated in the same way except for the aqueous phase, which contains both ES100 and pullulan in an optimized ratio with 2% PVA and 0.1 N NaOH

solution. The aqueous phase was devoid of methanol because highly soluble pullulan quickly precipitated in methanol, while ES100 was still able to dissolve in 0.1 N NaOH solution. The formed O/W nanoemulsion was kept stirred overnight for organic solvent evaporation. Afterwards, Dexa-GP/ES NPs, GP/Pu NPs, or GP/ES/Pu NCs were centrifuged (13,500 rpm, 40 min) for the removal of untrapped drug and residual solvents. Then the obtained pellets were mixed with cryoprotectant (5% trehalose) for freeze-drying at –80 °C. Finally, the dried white amorphous powder of GP/ES/Pu NCs were acquired and further used for characterization. Rhodamine-B dye loaded nanocargoes were prepared using the same methodology.

2.5. Physicochemical characterization

The HPLC method for drug quantification is mentioned in Supplementary Materials (Section 1.1). Physicochemical characteristics including particle size, zeta potential, PDI and conductivity of the prepared nanocargoes were determined through the Malvern zeta sizer ZS90 (Malvern Instruments, Worcestershire, UK). For particle morphology, a scanning electron microscope (SEM) (Hitachi S4700, Hitachi Scientific Ltd., Tokyo, Japan) provided a larger view. Drug entrapment efficiency (EE) and actual drug content (%) were measured at 240 nm under HPLC (Supplementary Materials, Section 1.2). Next, ATR-FTIR analysis was conducted to detect possible interactions among drug and excipients in a mixture or inside nanocargoes, using ATR Cary 630 FTIR (Agilent Technologies, USA). To investigate the thermal degradation behavior of the prepared nanocargoes, thermal gravimetric analysis (TGA) was performed in the range of 30–800 °C under a thermal gravimetric analyzer (Mettler-Toledo GmbH, Gießen, Germany). Further, the crystalline or amorphous nature of the drug, polymer and nanocargoes were evaluated through X-ray powder diffraction (XPRD) (Bruker[®] AXS GmbH, Germany). For stability assessment, nanocargoes were examined for morphological, physicochemical characteristics and drug content for six months according to ICH guidelines.

2.6. Drug release and kinetics

Drug release from GP/ES NPs, GP/Pu NPs and GP/ES/Pu NCs was estimated through the dialysis membrane diffusion method in simulated gastric fluid (SGF) of pH 1.2 for the first 2 h [27], then in phosphate buffer (pH 4.5) for the next 2 h to mimic acid-fed conditions, and then in simulated intestinal fluid (SIF, pH 7.4) with or without cecal contents (5%, w/v) [29], to match large intestine conditions for 72 h with sampling at regular time-period (Supplementary Materials, Section 1.3).

2.7. Mucin binding study

The extent of mucin-nanocargoes interaction was observed through UV spectrophotometry at 255 nm [30], and further determined through particle size analysis and viscoelastic effects using a cone-plate rheometer (CE AMETEK Brookfield, USA) by varying shear force [31]. (Supplementary Materials, Section 1.4).

2.8. *In vitro* biocompatibility, cell-uptake and permeation studies

In vitro biocompatibility of nanocargoes towards the RBCs was assessed through a hemolysis assay [27]. MTT assay was performed to check colon cells [32] and macrophages [33,34] cell viability and nanocargoes toxicity potential. (Supplementary Materials, Section 1.5i-ii)

Fluorescein dye loaded GP and GP/ES/Pu NCs were prepared to study *in vitro* uptake potential in peritoneal macrophages and colon cells using RPMI-1640 media in a controlled humidified 5% CO₂ environment at 37 °C. The nanocargoes were incubated for 2 and 4 h, washed to remove free dye, fixed, and visualized under a fluorescent microscope (Olympus CX41, Olympus Corporation, Japan). The fluorescence was quantified through ImageJ software (NIH, USA). Plain dye served as a control. To determine the involvement of the MGL-2 receptor in the cellular uptake of D-galactose anchored nanocarriers, we pre-treated macrophage cell culture with free D-galactose and then incubated macrophages with Dye-GP NPs.

In vitro permeation and retention of Rhodamine-B dye loaded GP/ES/Pu (Rho-GP/ES/Pu) NCs were determined using excised goat intestine through the sac method at 37 ± 1 °C and 50 rpm under a bath shaker. 1 ml samples were withdrawn from the outer buffer compartment at a periodic interval of 2, 4, 6 and 8 h and quantified at 560 nm under a UV-Visible spectrometer (Supplementary Materials, Section 1.5iii).

2.9. *In vivo* NCs targeting index and localization capacity in the DSS inflamed colon

After DSS induced development of colitis, mice were tested for nanocargoes targeting potential. After 6-h NCs administration, drug concentration was quantified in the stomach, small intestine, colon, spleen and the major organs to demonstrate NCs residence. DSS treated colitis mice ($n = 3$ / group) were administered either with DEXA-GP/ES/Pu NCs or with a plain DEXA drug through oral gavage at a same dose of drug separately. NCs colon targeting index ($C_{\text{nanocargoes}}/C_{\text{free drug}}$) and selectivity index ($C_{\text{colon}}/C_{\text{plasma}}$) were calculated [35]. The drug concentration in plasma was assessed after 24-h administration of either the plain DEXA or DEXA-GP/ES/Pu NCs using HPLC method. Flow Cytometer (BD, FACSTM, US) was used to investigate nanocargoes internalization by the colon-macrophages after 6-h intake (Supplementary Materials, Section 1.6.1-1.6.3).

2.10. *In vivo* therapeutic intervention of DSS induced colitis mice

To investigate the therapeutic effectiveness of DEXA-GP/ES/Pu NCs against DSS-induced colitis, mice were randomly distributed following protocols of minimum harm and ARRIVE guidelines into 4 groups ($n = 5$). The number of subjects was selected according to the animal resource equation [36] and considering ethical protocols of minimum harm (3Rs) [37].

Group I (Normal control): Normal healthy mice, received drinking water.

Group II (DSS): DSS-induced colitis mice (disease control), received 3% DSS in drinking water for 7 d.

Group III (DEXA/ free drug control): DSS-induced colitis mice after 7-d disease development received DEXA drug solution (dose= 5 mg/kg) through oral gavage, on Day 7-14.

Group IV (DEXA-GP/ES/Pu NCs): DSS-induced colitis mice after 7-d disease development treated with DEXA-GP/ES/Pu NCs (at dEXA dose equivalent to 5 mg/kg) through oral gavage, on Day 7-14.

2.11. Assessment of progression and intervention of colitis

Disease progression was monitored through physical manifestations including body weight loss, rectal bleeding and stool consistency, and cumulatively scored as a disease activity index (DAI). DAI was calculated according to the reported procedure [7]. Further, inflammation indices like colon morphometrics, colon weight-to-length ratio, and spleen weight were estimated to explore the extent of the disease. The mice mortality rate in each group was assessed for estimating mice survival after nanocargoes treatment.

2.12. Evaluation of colonic vascular integrity

Vascular integrity in IBD is compromised because of altered endothelial function in inflammation [38]. Vascular permeation was assessed through the Evans blue assay on the last day of the experiment. For method, see Supplementary Materials, Section 1.7.

2.13. Histopathological assessment

Small colon segments from all groups were fixed in 10% buffered formalin, paraffin-embedded, thin sliced with a microtome and stained with H&E. The stained samples were observed under a microscope and assessed on a scale of 0-12, based on inflammation extent and mucosal injury [39].

2.14. Immunohistochemistry

DEXA loaded GP/ES/Pu NCs mechanistic action on the expression of NF-κB, and COX-2 was evaluated through immunohistochemistry, according to the reported protocol [40,41]. Briefly, paraffin-embedded colon tissues were rehydrated through xylene and graded ethanol, followed by quenching with 3% H₂O₂ and incubation with 5% normal goat serum for 20 min. Then incubated with mouse anti-COX-2 and anti-NF-κB antibodies (Santa Cruz Biotechnology, Inc., USA) overnight. Next day, slides were treated with biotinylated goat anti-mouse secondary antibodies and ABC reagents (SCBT, USA); thereafter swept with 0.1 M PBS and stained with diaminobenzidine (DAB) (Sigma Aldrich, St. Louis, USA). Quantitative expression of COX-2 and NF-κB was computed through ImageJ software (NIH, USA).

2.15. ATR-FTIR of the colon tissues

Excised dried colon tissues were sliced into thin pieces and mounted on the specimen holder [42]. Subsequently, tissues were analyzed in the range of 400–4000 cm^{-1} wavenumber under ATR-FTIR to detect structural and functional changes in the colon before and after disease induction and nanoparticle treatment.

2.16. Evaluation of colon microbial content

To determine colon microflora alterations after induction of colitis and to elucidate the effect of nanoparticle treatment on restoration of the microbiome, colon feces samples from all groups were obtained at the end of the experiment. Bacterial colonies from the feces were incubated in the nutrient agar plate at 37 °C, and colony forming units (CFU) were counted after 24 h using the Galaxy 230 colony counter instrument. Results were expressed as log CFU/ml \pm SD ($n = 3$).

2.17. Real-time PCR (RT-PCR) and ELISA

Expression of proteins that regulate tight junction function (E-Cadherin), and mucosal injury (iNOS) was estimated through RT-PCR analysis using a Magnetic Induction Cycle PCR (Bio Molecular System, Australia) machine (Supplementary Materials, Section 1.8, Table S1). The amount of pro-inflammatory cytokines, tumor necrosis factor-alpha (TNF- α) and interleukin-6 (IL-6) were determined in the excised colon tissues from each mice group using commercially available ELISA kits (eBioscience, Inc., CA, USA) according to the manufacturer's directions.

2.18. Biochemical antioxidant assays and hematology

The levels of antioxidant enzymes including GSH, GST and catalase [7], and oxidative species including lipid peroxidation (LPO)-malondialdehyde (MDA), and nitrite (NO) concentrations were assessed in the colon sections [43]. Myeloperoxidase MPO activity was determined through the CTAB buffer method [44] (Supplementary Materials, Section 1.9). Hematological parameters were estimated from the blood derived from the experimental groups. The effect of Dexa loaded nanocargoes on blood glucose was tested using EasyGlucTM (Infopia, Korea) test strips.

2.19. In vivo biocompatibility and toxicity investigations

BALB/c healthy male mice, weighing 25–30 g, were tested under pathogen-free standard laboratory conditions with *ad libitum* access to food and water. Mice were orally administered with Dexa-GP/ES/Pu NCs (drug dose = 5 mg/kg) for 7 d to explore the possible toxic effects of nanocargoes inside the living system. A control group of mice received plain water only. Mice were assessed daily for acute toxicity symptoms including body weight loss, mortality rate, and behavioral patterns like anxiety or distress lethargy, pain, disturbance in food and water intake, sleep, and defecation [28]. After 7 d, mice were euthanized and assessed for

organ-to-body weight ratio, histology of the vital organs, and hematological parameters.

Since colon is the major targeting organ, colon tissues were evaluated for the nanocargoes effects on cellular death through apoptotic analysis under flowcytometry (BD, FACSTM, USA) using Annexin-V and propidium iodide dyes. Single-cell suspensions were analyzed for viability, apoptosis, and necrosis with FACS scan using the Cell Quest software (BD, Bioscience, San Jose, CA, USA).

2.20. Statistical analysis

All the data is represented as mean \pm SD, unless otherwise stated. Student's *t*-test followed by one-way ANOVA was performed for the statistical comparison between groups. The level of significance was considered 0.05 ($P < 0.05$), 0.01 ($P < 0.01$) and 0.001 ($P < 0.001$).

3. Results and discussion

3.1. Synthesis of polymer and nanocargoes and characterization

The GP polymer was synthesized successfully through the esterification reaction and confirmed using ATR-FTIR and ¹HNMR [27]; the spectral ranges can be found in (Supplementary Materials, Section 2.1).

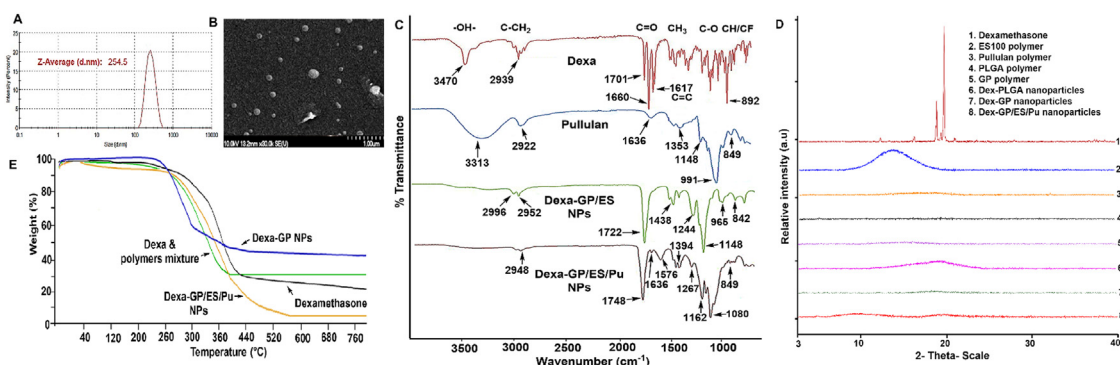
Dexa-GP NPs were prepared through the modified O/W emulsion method with the desired attributes. Next, Dexa-GP NPs coating with ES100 and pullulan produced Dexa-GP/ES/Pu NCs having both pH sensitive and microbial sensitive characteristics. For coating, ES100 to pullulan concentrations were pre-assessed, and the ES/Pu ratio of 2:1 was considered based on minimal dose dumping at pH 1.2.

The prepared Dexa-GP/ES/Pu NCs (2:1) have particle size of around 254.23 ± 1.95 nm, zeta potential of -27.6 ± 0.115 mV, and PDI of 0.147 ± 0.018 (Table 1, Fig. 1A and B), which satisfy the demands to target inflamed mucosa and epithelial cells of the large intestine with enhanced sensitivity to pH and microbial content. Zeta potential confirmed the presence of an anionic ES100 coat on Dexa-GP/ES/Pu NCs. The Dexa-GP/ES NCs found to be more negatively charged than Dexa-GP/ES/Pu NCs, possibly because of the pullulan content in the later (Table 1). The monodispersed nanosystem possessed the correct properties to avoid gastric pH degradation (pH 1.2) and stability against gastric enzymes.

Moreover, SEM analysis revealed a spherical smooth morphology of the Dexa-GP/ES/Pu NCs with particle sizes ranging around 100–200 nm, consistent with zeta sizer findings (Fig. 1B). ATR-FTIR evaluation of drug, polymers, and nanocargoes negate presence of polymer-polymer or drug-polymer interactions. Furthermore, FITR spectra obtained for Dexa-GP/ES/Pu NCs confirmed complete entrapment of the drug inside the polymeric structure and absence of any surface-bound or untrapped drug on the surface (Fig. 1C). The XPRD suggested Dexa conversion into an amorphous form when entrapped in the polymeric nanocargoes with low intensity peaks (Fig. 1D), while plain

Table 1 – Physicochemical characteristics of Dexa loaded nanocargoes (mean \pm SD, $n = 3$).

Formulation	Particle size (nm)	Zeta potential (mV)	PDI	EE%	DL (ug/mg)	Yield (%)	Conductivity (mS/cm)
Dexa-GP NPs	118.77 \pm 0.74	-9.5 \pm 0.19	0.064 \pm 0.004	89.97 \pm 0.4	81.79 \pm 0.35	89.2 \pm 3.7	0.0374 \pm 0.000115
Dexa-GP/ES NPs	189.57 \pm 0.865	-34.9 \pm 0.611	0.228 \pm 0.0132	92.64 \pm 3.5	43.77 \pm 1.705	89.33 \pm 1.38	0.0596 \pm 0.000611
Dexa-GP/Pu NPs	213.067 \pm 0.5	-10.83 \pm 0.154	0.059 \pm 0.015	91.97 \pm 3.36	43.32 \pm 1.6	90 \pm 3.21	0.0709 \pm 0.00025
Dexa-GP/ES/Pu NCs (1:1)	200.667 \pm 4.8	-22.52 \pm 0.155	0.252 \pm 0.0023	92.76 \pm 2.7	44.17 \pm 1.3	91.41 \pm 3.75	0.056 \pm 0.00015
Dexa-GP/ES/Pu NCs (2:1)	254.23 \pm 1.95	-27.6 \pm 0.115	0.147 \pm 0.018	94.56 \pm 1.6	45.78 \pm 1.7	91.83 \pm 3.4	0.058 \pm 0.000154

**Fig. 1 – Physicochemical characterization of Dexa-GP/ES/Pu NCs. (A) Particle size analysis, (B) SEM analysis, (C) ATR-FTIR, (D) XPRD, and (E) TGA analysis of drug, excipients and nanocargoes.**

Dexa exists in the crystalline form as indicated through sharp peaks in the spectrum. Polymers including PLGA, GP, ES100 and pullulan are amorphous in nature, as shown in the XPRD spectra (Fig. 1D). Thermal withstanding of nanocargoes was assured through TGA investigations (Fig. 1E). It demonstrated that Dexa inside the polymeric nanocargoes attained enhanced thermal stability as compared to its free form.

Lyophilized Dexa-GP/ES/Pu NCs were evaluated for physicochemical characteristics after 1 and 6 months of storage at 4 °C and 25 °C. Nanocargoes retained the particle size, zeta potential, PDI, and EE within the acceptable limits (Table S2). Further, Dexa-GP/ES/Pu NCs were dispersed in SIF (pH 7.4) with or without cecal contents. After 72 h of incubation, the particles were within the size limits, the PDI was lower, and the zeta potential was representative of GP NPs because of the dissolution of ES100 and pullulan coat at pH 7.4 which is the threshold to dissolve the enteric coat (Table S3).

3.2. Drug release and kinetics

Dexa release from GP/ES/Pu NCs was determined through the dialysis diffusion method in SGF (pH 1.2), PBS (pH 4.5) and SIF (pH 7.4). The range of pH was selected because of variations across the GIT; the acidic range over pH 1.2–4.5 covers the upper GIT including stomach and upper region of small intestine, while pH 7.4 is specific to colon [3]. In comparison, Dexa release from GP/ES and GP/Pu NPs was studied to elucidate the effect of dual ES/Pu coat on drug release at colon. Moreover, drug release in the presence of cecal contents (5%, w/v) was observed to simulate the colonic

microenvironment. At pH 1.2 (0–2 h), GP/Pu NPs released 25.3%–29.6%, GP/ES NPs exhibited 9.8%–11.8%, and GP/ES/Pu NCs released 4.3%–7.2% (Fig. 2A). At pH 1.2, dual GP/ES/Pu NCs had significantly reduced the burst release of the drug at 30 min (** $P < 0.01$), 1 h (** $P < 0.01$), and 2 h (** $P < 0.01$), in comparison to GP/Pu NPs. While non-significant difference was observed in the drug release behavior between dual GP/ES/Pu NCs and GP/ES NPs ($P = NS$ at 0–2 h) at pH 1.2. However, at pH 4.5, GP/ES/Pu NCs markedly reduced the drug release, in comparison to both GP/Pu (** $P < 0.001$) and GP/ES NPs (** $P < 0.001$, Fig. 2A), depicting that dual stimuli sensitive nanocargoes provides better stability at both pH 1.2 and 4.5. At pH 7.4, drug release from GP/Pu, GP/ES and GP/ES/Pu NCs was parallel and sustained, with approximately 82.5%, 84.3%, and 83.5% drug release at 72 h, respectively (Fig. 2A).

In SIF (pH 7.4) with cecal contents, GP/Pu NPs released approximating 90%, GP/ES NPs released about 81% and GP/ES/Pu NCs had 86% drug release within 72 h (Fig. 2B). Addition of cecal content in SIF (pH 7.4) affected the drug release from nanoparticles with the pullulan coat (GP/Pu NPs) because cecal contents are the source of microbial enzymes that consume pullulan. Thus, cecal contents majorly affect drug release from GP/Pu NPs and moderately affect drug release from GP/ES/Pu NCs, while having negligible effects on GP/ES NPs drug release (Fig. 2B).

Kinetics for GP/ES NCs and GP/Pu NCs are mentioned in Supplementary Materials, Section 2.3, Table S4 and S5. Dexa-GP/ES/Pu NCs drug release kinetics were fitted to the Peppas-Sahlin model at acidic pH and pH 7.4, both in the presence and absence of cecal contents. The values of Korsmeyer's 'n' and Peppas-Sahlin 'm' are greater than 0.5 at acidic pH, which means non-Fickian drug release mechanism. Whereas

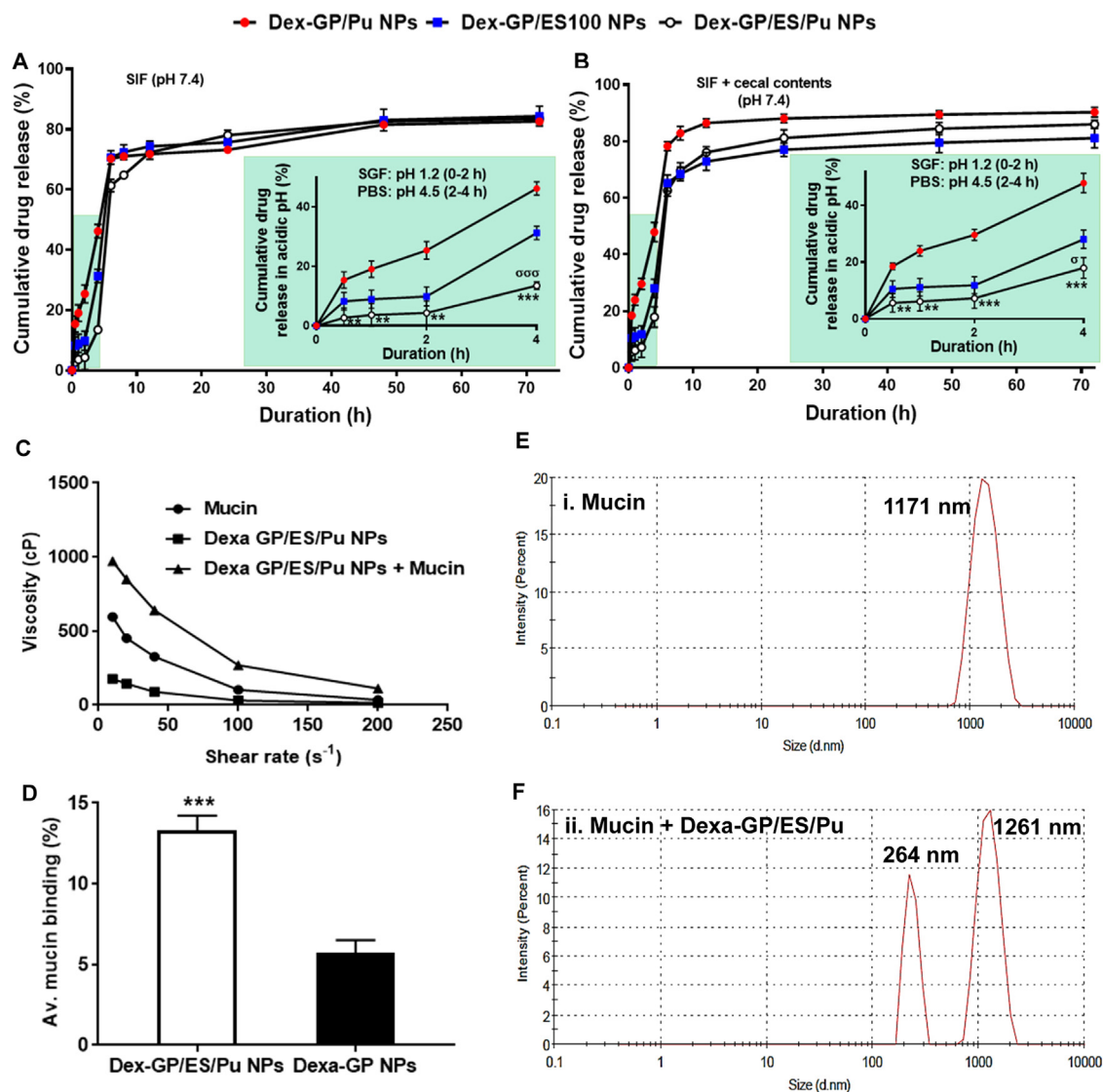


Fig. 2 – Dexa release from GP/Pu NPs, GP/ES NPs and GP/ES/Pu NCs ($n = 3$) at acidic pH (pH 1.2–4.5) and pH 7.4, without or with cecal contents (A, B) (Note: Dexa-GP/ES/Pu NCs vs GP/Pu NPs: $*P < 0.05$, $P < 0.01$, $***P < 0.001$; and Dexa-GP/ES/Pu NCs vs GP/ES NPs: $\sigma P < 0.05$, $\sigma\sigma P < 0.01$, $\sigma\sigma\sigma P < 0.001$); Rheological investigations of mucin and nanocargoes interaction (C); Spectrophotometric analysis of percent mucin binding to nanocargoes (D); Size analysis of Mucin (E); Size analysis after mucin-nanocargoes interaction (F).**

the values are lesser than 0.5 at pH 7.4 (\pm cecal material) which describes Fickian diffusion of drug to move outside the polymeric nanocargoes (Supplementary Materials, Section 2.3, Table S6). Both Korsmeyer and Peppas-Sahlin described drug release from polymers and polymeric nanoparticles either because of polymer chain elongation, diffusion or both mechanisms [27]. Overall, non-Fickian was the main mechanism of drug release at acidic pH because the drug had to pass through the core and outward enteric coat which involves polymer relaxation and elongation in the release process. While the major drug release mechanism at pH 7.4 is Fickian diffusion (Supplementary Materials, Section 2.3, Table S6), that negates polymer relaxation because the outer enteric coat already dissolved at the threshold pH that uncovered the GP nanocore, from where the drug released through a diffusion process.

3.3. Mucin binding study

The rheological investigations of the mucin-nanocargoes mixture suggested an increase in viscosity compared to Dexa-GP/ES/Pu NCs or mucin alone. The consistent viscosity increase was observed at different shear rates (10–200 s^{-1}) at a fixed mucin-nanocargoes concentration (1:1) (Fig. 2C). The rheological synergism is the mucoadhesion evaluation parameter for the polymeric systems [45]. The synergism findings showed viscosity for mucin-formulation mixture (η_{mix}) was higher than the $\eta_{NCs} + \eta_{muc}$ values, thus indicating positive rheological synergism.

Rheological studies indicated interaction between mucin and Dexa-GP/ES/Pu NCs. To further elucidate, the extent of mucin binding was explored. It was found that the binding efficiency of mucin to Dexa-GP/ES/Pu NCs was about 13.3%,

compared to 5.7% binding with Dexa-GP NPs, indicating a 2-fold higher interaction in the presence of ES100 and pullulan coat on GP NPs (Fig. 2D). Though the enteric coat increased the mucin interaction, the percent binding was still not high enough. Further, particle size distribution analysis of the mucin-nanocargoes mixture revealed the presence of bimodal peaks, because of nanocargoes (264 nm) and mucin (1261 nm). The size of nanocargoes showed insignificant differences ($\sim 10\text{--}20$ nm, $P = 0.09$ (NS)) after incubation with mucin, pointing to the little mucin adsorption on the surface due to the anionic nature of the GP/ES/Pu NCs (Fig. 2E and F). Together, findings suggested that polymethacrylate and pullulan-based coatings improved mucoadhesion to some extent because of the swelling properties of the polymers [46,47]. However, the anionic nature of the system prevented extensive mucin binding [48,49].

3.4. In vitro biocompatibility studies

3.4.1. Hemolysis assay

RBCs hemolytic activity of Dexa-GP NPs, Dexa-GP/ES NPs and Dexa-GP/ES/Pu NCs at drug concentrations of 25–100 $\mu\text{g/ml}$ demonstrated that all formulations were safer and negated the potential for blood toxicity. At all concentrations, hemolysis was less than 2% for Dexa-GP/ES NPs and less than 1% for Dexa-GP and Dexa-GP/ES/Pu NCs (Fig. 3A and B). The presence of pullulan in the enteric coat further enhanced the safety profile of the nanosystem.

3.4.2. Cellular biocompatibility (MTT)

MTT cellular viability assessment of Dexa-GP NPs, and Dexa-GP/ES/Pu NCs on elicited macrophages and murine-colon cells after 24 and 48 h demonstrated the nontoxic, biocompatible nature of the drug loaded formulations. In fact, Dexa free state exhibited lesser cell viability than those encapsulated within polymeric nanosystems. Dexa drug have significantly reduced cellular viability when compared with normal control. Both nanosystems have proven to be biosafe, with $>80\%$ macrophage viability and $>70\%$ colon-cells viability at various concentrations of drug after 24 and 48 h, and were found to differ insignificantly from the normal control. Dexa-GP/ES/Pu NCs at various concentrations have shown macrophage cell viability of about 88%–95% and 83%–91% (Fig. 3C and 3D) and colon-cell viability of 77%–86% and 74%–83% after 24 and 48 h, respectively (Fig. 3E and F).

3.5. In vitro cell-uptake studies

Fluorescein isothiocyanate loaded GP NPs and GP/ES/Pu NCs were incubated with murine derived macrophages to visualize the cellular endocytosis of nanocargoes loaded with fluorescent dye (Fig. 3G and H). Free dye was used as a control. Dye loaded GP NPs and GP/ES/Pu NCs showed fluorescence after 2 and 4 h of incubation. Dye-GP/ES/Pu NCs have maximum uptake intensity after 4 h (Fig. 3G and H), because ES/Pu coat dissolution or disintegration over the time exposes the underneath GP core, which have more binding affinity for the MGL-2 macrophage-surface receptor leading to increased cellular uptake after 4 h. Dye-GP NPs have slightly

more uptake than Dye-GP/ES/Pu NCs because of their small size and exposed ligand on the surface, while GP/ES/Pu NCs take some time for enteric coat dissolution.

The mechanistic evaluation demonstrated that the presence of free D-galactose in the media competitively inhibited the uptake of Dye-GP NPs, as depicted through diminished uptake fluorescence (Supplementary Materials, Section 2.4, Fig. S1). The findings suggested the role of the MGL-2 receptor in the cellular uptake of Dye-GP NPs.

In colon cells, both types of nanoparticles had extensive internalization by the colon cell membranes (Fig. 3G and H). The increased uptake was based on the fact that particles around 200 nm are easily taken up by the epithelial cells under enhanced epithelial permeability and retention effect (eEPR) [50].

3.6. In vitro permeation and retention assay

In vitro permeation assay was performed to evaluate the permeation and retention effect of Rho-GP/ES/Pu NCs across goat intestine, over a period of 8 h in PBS (pH 7.4) at 37 °C (Fig. 4A-D). The greatest retention was observed after 4 h of Rho-GP/ES/Pu NCs incubation. When compared with the free Rhodamine-B control, it was clear that nanocargoes exhibited significantly higher retention (Fig. 4B), lower permeation (Fig. 4C) and high retention-to-permeation ratio (Fig. 4D) at all time points and incur sustained release characteristics, as manifested through increased concentration and fluorescence of dye in the intestine with lesser permeability into the buffer (Fig. 4B-D). The asterisks in Fig. 4B-D define level of statistical significance at each time point. Rhodamine-B encapsulation within the nanocarrier system retained within the intestinal tissue for a long time. This experiment further demonstrated enhanced local retention of the GP/ES/Pu NCs in the intestine.

3.7. In vivo nanocargoes targeting index and localization capacity in the inflamed colon

After establishment of DSS-colitis, mice were randomly divided for the targeting studies ($n = 3$) and therapeutic studies ($n = 5$). Dexa-GP/ES/Pu NCs localization in healthy and DSS-induced inflamed mice after 6 h of oral administration was investigated. Drug released from the nanocargoes in a sustained fashion, and thus retained in the colon for a prolonged time. Therefore, the estimation of drug concentration at the colon was an indirect measure of nanocargoes localization. It was found that the percent drug retention in the inflamed colon was significantly higher ($P < 0.01^{**}$) than the drug concentration in the healthy colon (Fig. 4E), because of altered pathophysiology in the inflammation including the eEPR effect, immune cells uptake, mucus, and majorly the MGL-2 involvement that contributed towards nanocargoes localization.

Further, nanocargoes' drug targeting capability and biodistribution were assessed through drug quantification in the GIT regions and vital organs. After 6 h of Dexa-GP/ES/Pu NCs administration to the DSS-induced colitis mice, the highest amount of drug accumulated in the colon ($\sim 41\%$), followed by plasma ($\sim 32\%$). Other organs (stomach, spleen,

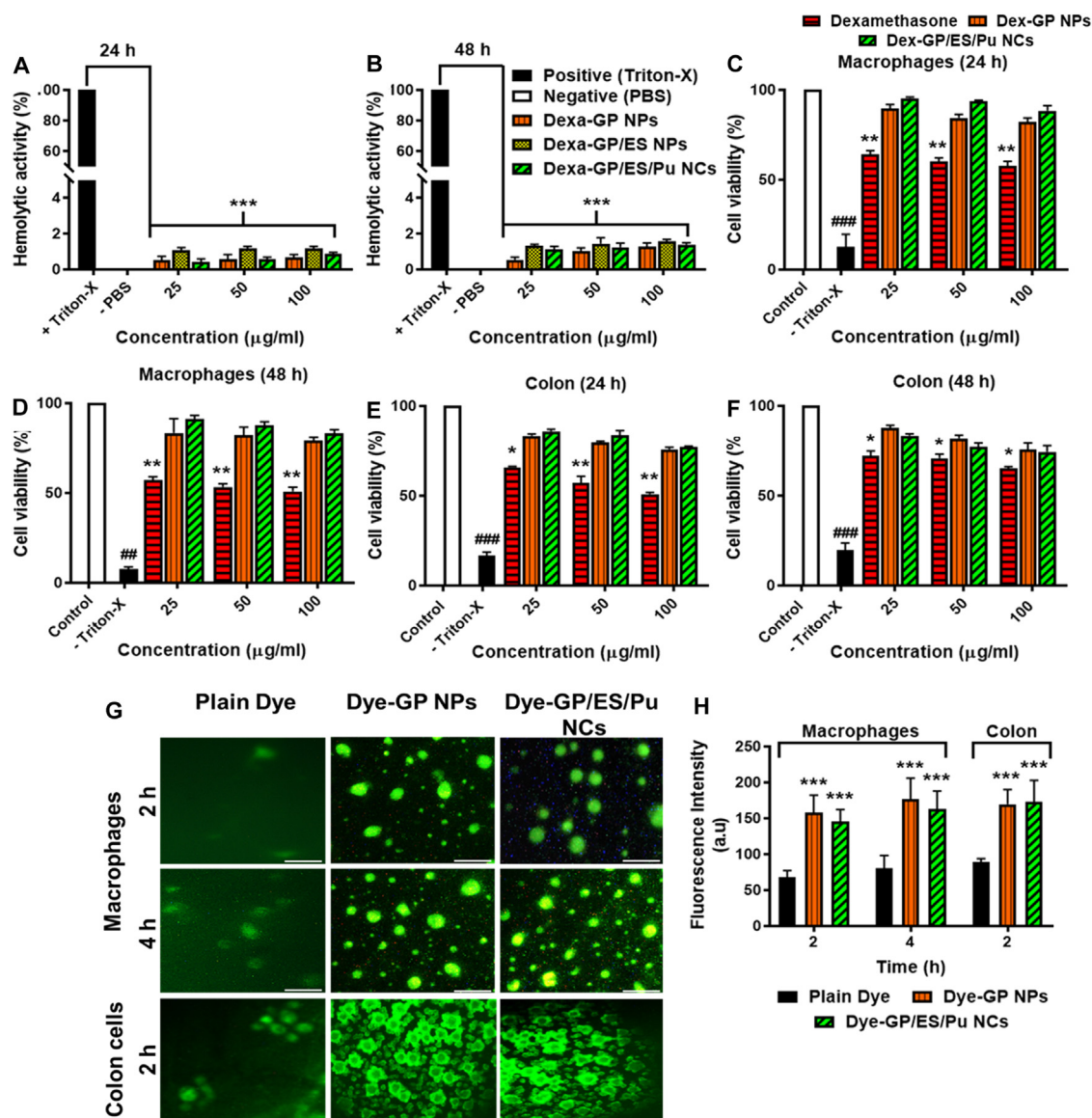


Fig. 3 – Hemolytic activity of nanoformulations after 24 h (A) and 48 h (B) ($n = 3$, Statistical significance between nano-formulations and Triton-X if $*P < 0.05$, $**P < 0.01$, $***P < 0.001$); Macrophage cell viability assay after 24 h (C) and 48 h (D); Colon cell viability assay after 24 h (E) and 48 h (F), (For C-F: $n = 3$; Statistical significance between nano-formulations and Normal cells control if $*P < 0.05$, $**P < 0.01$, $***P < 0.001$ and between Triton-X and Normal control if $*P < 0.05$, $**P < 0.01$, $***P < 0.001$); Macrophage and colon cells uptake of dye-labelled nanoformulations ($n = 3$) (G), Fluorescence intensity of the dye-labelled nanoformulation up taken by the macrophage and colon cells, scale = 25 μm (H), ($n = 3$; Statistical significance between nano-formulations and plain dye control if $*P < 0.05$, $**P < 0.01$, $***P < 0.001$).

small intestine, liver, kidney) had only a small portion of the drug after nanocarriers intake (Fig. 4F). While the free drug, given to the control group, failed to localize in the colon (~2.6%) and was found primarily in the plasma (~79%). The nanocarriers led colon targeting index was calculated to be 16.633 ± 3.5 , and the selectivity index was 1.29 ± 0.04 , which indicated the site-specificity and drug targeting ability of the nanocarriers (Fig. 4F). Thus, we postulate that the dual microbial-pH sensitive enteric layer on nanocarriers gets dissolved in the colon microenvironment, slowly disclosing

the underneath drug containing GP core which binds to MGL-2 receptors on colonic macrophages and releases the payload in a sustained manner.

FCS analysis was performed to elucidate the uptake of dye loaded GP/ES/Pu NCs by the macrophages derived from inflamed colon lamina propria. The analysis showed a right shift in the forward scattering (FSC-H-FITC) and an upward shift in the SSC-H plot, constituting the R1 area (Fig. 4H). The scattering depicted changes in the morphology and size of the macrophage cells which highlighted the cellular uptake

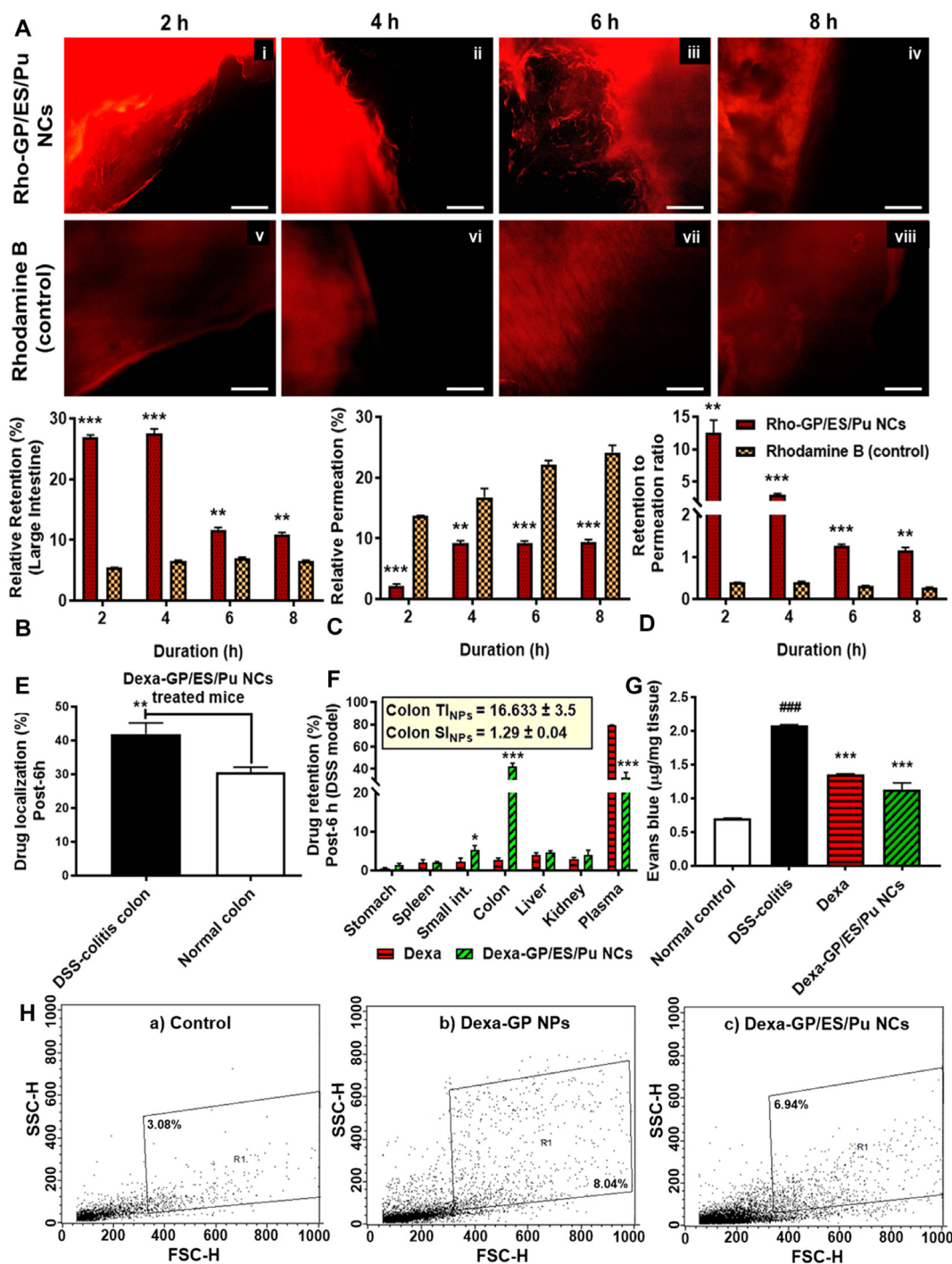


Fig. 4 – (A) Cross section of goat intestine illuminating under dye released from Rho-GP/ES/Pu NCs retention (i-iv) and free Rho dye control (v-viii) over 8 h, scale = 100 µm; **(B)** Relative percentage retention in the large intestine; **(C)** Relative percentage permeation across intestine into the buffer (pH 7.4); **(D)** Retention to permeation ratio of the Rho-GP/ES/Pu NCs and free dye for 8 h. (B-D: n = 3; Statistical significance between Rho-GP/ES/Pu NCs and free Rho if *P<0.05, **P<0.01, ***P<0.001); **(E)** Percentage drug localization after 6-h administration of Dexa-GP/ES/Pu NCs to the inflamed (DSS-induced colitis) and normal mice (n = 5; Statistical significance between DSS and Normal group if *P<0.05, **P<0.01, ***P<0.001); **(F)** Percentage drug retention or biodistribution to the vital organs after 6-h administration of Dexa-GP/ES/Pu NCs, n = 5; Statistical significance between Dexa-GP/ES/Pu NCs and Dexa*P<0.05, **P<0.01, ***P<0.001); **(G)** Vascular integrity test: Evans blue permeation across vessels into the inflamed colon (n = 3; Statistical significance between treated mice Vs DSS-colitis group if *P<0.05, **P<0.01, ***P<0.001 and Normal vs DSS: *P<0.05, ##P<0.01, ###P<0.001); **(H)** Flowcytometry to analyze fluorescein loaded GP/ES/Pu NCs uptake by the colon-derived macrophages, untreated control (a), GP treated (b), GP/ES/Pu NCs treated (c) (n = 3).

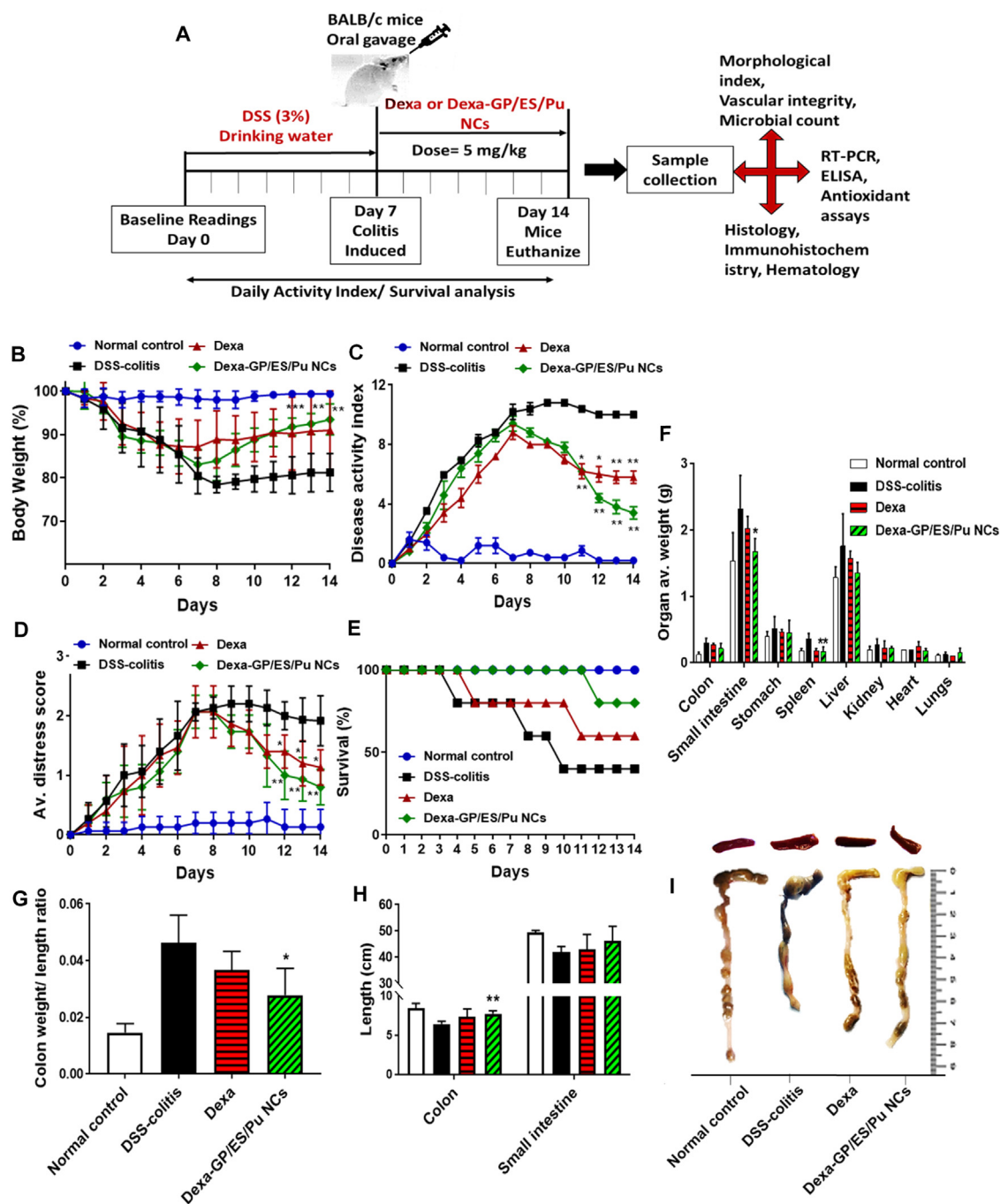


Fig. 5 – Therapeutic evaluation of Dexa-GP/ES/Pu NCs; Scheme of experimental design (A), body weight assessment (B), DAI scores (C), vital organs weight assessment (F), distress scores (D) and mortality (E), colon weight to length ratio (G), length of intestines (H), pictorial representation of colon and spleen (I). For statistical significance between treatment groups vs DSS colitis: * $P < 0.05$, ** $P < 0.01$, *** $P < 0.001$; the significance levels were same for Normal VS DSS-colitis except asterisks were changed to sign# ($n = 5$).

of nanocarriers. A control group of untreated macrophage cells was run in parallel. It was noted that GP NPs had slightly more internalization than GP/ES/Pu NCs because the galactose ligand in the GP NPs was exposed, therefore directly bound to the MGL-2 receptor of macrophages [27]. However, GP/ES/Pu NCs uncover the GP core over time and have more long-lasting uptake potential.

3.8. Oral delivery of Dexa-GP/ES/Pu NCs for therapeutic intervention of DSS induced colitis

3.8.1. Assessment of progression and intervention of colitis through morphological parameters and mortality rate
In vivo experimental design to investigate the therapeutic efficacy of nano-formulation is presented in Fig. 5A.

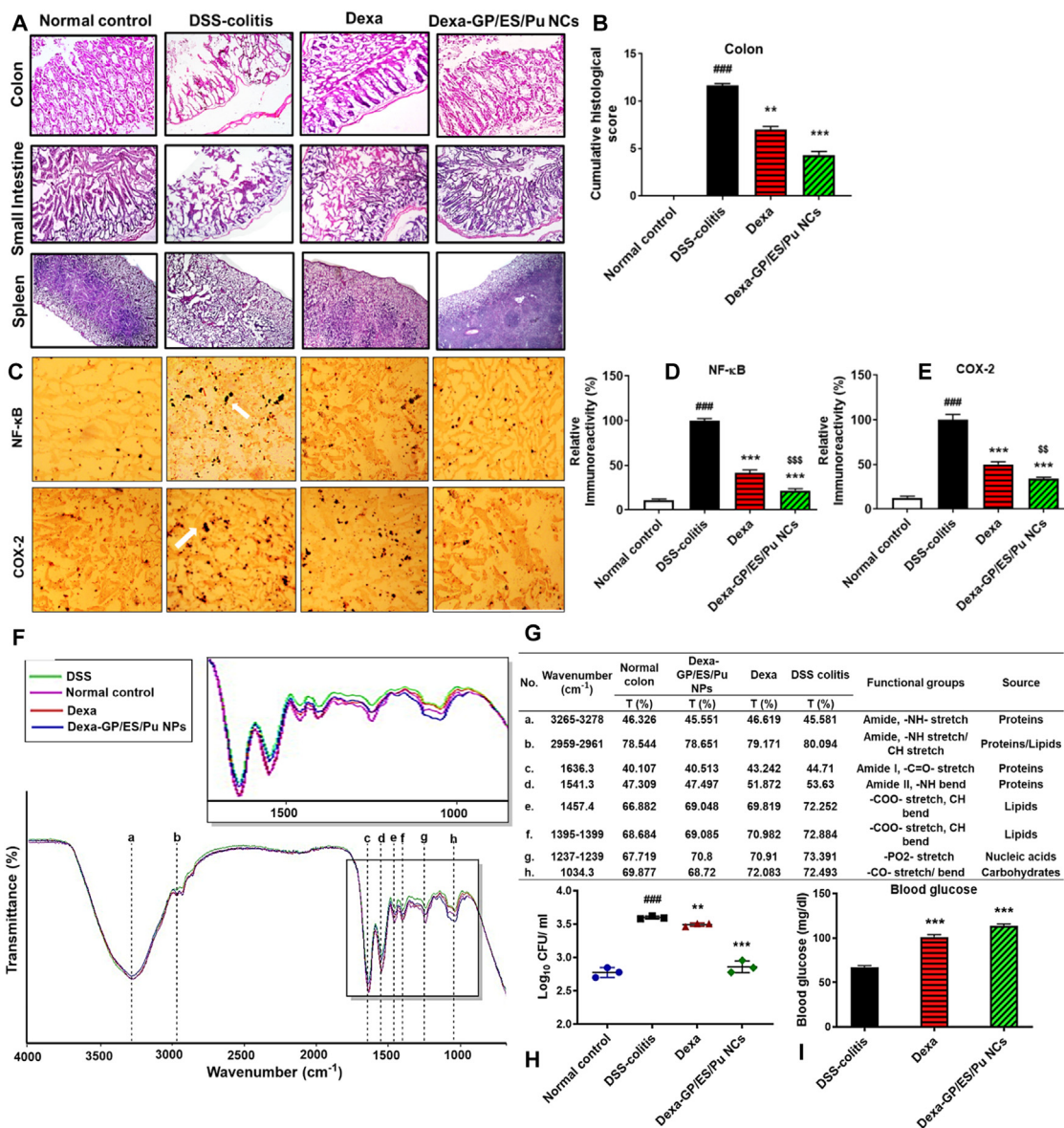


Fig. 6 - (A) Histology of colon, small intestine, and spleen from the representatives of normal control, DSS-colitis, Dexa and Dexa-GP/ES/Pu NCs treated mice groups (scale = 100 μ m); **(B)** Colon cumulative histopathological score, $n = 3$; **(C)** Expression of NF- κ B and COX-2 at the colon tissues in the normal control, DSS-colitis, Dexa and Dexa-GP/ES/Pu NCs treated groups by immunohistochemistry, $n = 3$; **(D)** Relative immunoreactivity (%) of NF- κ B; **(E)** Relative immunoreactivity of COX-2; **(F)** ATR-FTIR spectra of colon tissues excised from normal control, DSS-colitis, Dexa and Dexa-GP/ES/Pu NCs treated groups, $n = 3$; **(G)** Descriptive analysis of ATR-FTIR peaks with percent transmittance at a particular wavenumber (cm⁻¹) and functional groups; **(H)** Microbial colony forming units (logCFU/ml) from the fecal suspension obtained from different groups under investigation, $n = 3$ /group; **(I)** Blood glucose levels of the mice of different groups under study, $n = 3$. Statistical significance between treatment groups and DSS colitis is defined as * $P < 0.05$, ** $P < 0.01$, *** $P < 0.001$; the significance levels between Normal control and DSS-colitis are # $P < 0.05$, ## $P < 0.01$, ### $P < 0.001$.

Progression of the disease was monitored daily. DSS induced colitis group developed signs of disease throughout the experiment (1–14 d), manifested through significant body weight decline at Day 14 ($t = 1.53 \times 10^{-5}$, ### $P < 0.001$), and highest DAI scores (DAI = 10.0 ± 0.23 , $t = 2.57 \times 10^{-5}$, ### $P < 0.001$) as compared to the normal control (DAI = 0.2 ± 0.12) (Fig. 5B and C). At the end, treatment with Dexa-GP/ES/Pu NCs recovered mice body weight up to

93.45% ($t = 0.00081$, *** $P < 0.001$), and lowered DAI score to 3.4 ± 0.41 ($t = 0.0013$, $P < 0.01$ **), as compared to DSS-colitis mice (Fig. 5B and C). Further, the distress monitoring revealed that colitis induced significant stress to the mice ($t = 0.00014$, ### $P < 0.001$) compared to normal; and treatment with both Dexa ($t = 0.0134$, * $P < 0.05$) and Dexa-GP/ES/Pu NCs ($t = 0.00225$, ** $P < 0.01$) alleviated the anxious symptoms of the colitis mice (Fig. 5D). Further, Dexa-GP/ES/Pu NCs treated mice had an

improved survival rate (80%), in comparison to untreated colitis mice (40%) (Fig. 5E).

Weight evaluation of the stomach, heart, liver, kidney, and lung showed that DSS induced colitis did not impinge on these organs, and thus treatment had no effect on these vital organs (Fig. 5F). Colon weight to length ratio, colon length and spleen weight index demonstrated that Dexa-GP/ES/Pu NCs recovered the inflammation indices of colitis mice towards normal values with a decline in colon weight to length ratio, an increase in colon length, and a reduction in splenic weight (Fig. 5F-I). It was observed that small intestine weight was significantly restored by the nanocargoes ($t = 0.04$, $*P < 0.05$) (Fig. 5F), while length was recovered to a small extent (Fig. 5H and I). Assessment of morphological parameters demonstrated improvement with the course of nanocargoes treatment.

3.8.2. Evaluation of colonic vascular integrity

Colon inflammation precedes structural and functional damage to the vascular endothelium by influencing cell adhesion molecules (CAMs), increasing leukocyte diapedesis, and regulating cytokines and mediators like NO, VEGF, etc. [50]. Therefore, the estimation of Evans blue permeation across the endothelial membrane to the colon indicated the extent of inflammation. Findings demonstrated that the highest amount of Evans blue was concentrated in the DSS induced colitis mice, and treatment with Dexa and Dexa-GP/ES/Pu NCs markedly decreased the dye permeation at the colon (Dexa-GP/ES/Pu NCs vs DSS: $t = 9.14 \times 10^{-5}$, $*** P < 0.001$) (Fig. 4G). Thus, treatment aided in the restoration of the endothelial integrity of the inflamed colon because of the recovery of epithelial integrity and chemokine factors.

3.8.3. Histopathological assessment

Histo-morphologic assessment enumerates loss of epithelial integrity, crypt distortion and immune cell infiltration with a cumulative damage score. DSS-induced colitis produced severe histological destruction (score: 11.66 ± 0.192 , $t = 3.98 \times 10^{-6}$, $###P < 0.001$ vs normal) (Fig. 6A and B). Dexa restored the total colon damage to a histology score of 7 ± 0.33 ($t = 0.0022$, $**P < 0.01$), while Dexa-GP/ES/Pu NCs have substantially alleviated the inflamed colon to a score of 4.33 ± 0.385 ($t = 0.00059$, $***P < 0.001$) (Fig. 6A and B).

The histopathological analysis of the small intestine depicted some signs of inflammation with altered villi-crypt ratio in the DSS-colitis groups; and the spleen has major marks of distortion, especially in the central white pulp region (Fig. 6A). Treatment with Dexa-GP/ES/Pu NCs recovered inflammation associated disruptions in the small intestine and spleen (Fig. 6A).

3.8.4. Immunohistochemistry

Since DSS-induced colitis increased the expression of inflammatory proteins and activated signaling pathways like MAPK and NF- κ B [51]. Therefore, the therapeutic efficacy of an anti-COX encapsulated drug (Dexa) inside the nanoformulation was investigated through immunohistochemical analysis of inflammatory signaling proteins. Findings indicated down-regulated expression of NF- κ B proteins by Dexa (~41%) and Dexa-GP/ES/Pu NCs (~21%)

and decreased expression of COX-2 protein on treatment with Dexa (~50%) and Dexa-GP/ES/Pu NCs (~33%) (Fig. 6C-E).

3.8.5. ATR-FTIR analysis of the colon tissues

The ATR-FTIR spectra obtained from pat dried colon tissues of different groups have been shown in Fig. 6F and G. While differentiating regions of the FTIR spectrum, the sub-ranges representing the N-H stretch of proteins are present in $3200\text{--}3300\text{ cm}^{-1}$. And amide I and amide II correspond to 1640 cm^{-1} and 1540 cm^{-1} , respectively. Lipidic domains are peaking around $2850\text{--}2960\text{ cm}^{-1}$ and $1390\text{--}1457\text{ cm}^{-1}$. The nucleic acid peak can be visualized at 1239 cm^{-1} , while carbohydrates are assigned to $1034\text{--}1100\text{ cm}^{-1}$ (Fig. 6F). These findings were consistent with the literature [52–54]. The major peak positions are almost the same in the normal and colitis tissues; however, the differences in peak intensity, transmittance, and shape reflect the deviations [53]. The structure and composition disruptions in the major biomolecules including proteins, lipids, nucleic acids and carbohydrates have an impact on the relative intensity exhibited by the functional groups of each biomolecule. The treatment with Dexa-GP/ES/Pu NCs was found to be fruitful in balancing all bio-molecular FTIR peaks representing protein amides, lipids, nucleic acid content, and carbohydrates because nanocargoes healed mucosal injury with restoration of structures, DNA/RNA, and mucin (Supplementary Materials, Section 2.5).

3.8.6. Evaluation of colon microbial content

DSS induction disturbed the microbial flora of the gut because of severe epithelial and luminal distortions [55]. The bacterial log CFU/ml in the fecal culture of DSS-colitis mice exceeds 1.3 folds than that of normal healthy mice ($P < 0.001$). Dexa and Dexa-GP/ES/Pu NCs treated mice have decreased fecal CFU to 3.49 ± 0.025 ($P < 0.01$ vs DSS) and 3.17 ± 0.029 ($P < 0.001$ vs DSS), respectively, demonstrating the effect of treatment in restoring the natural microbiome (Fig. 6H).

3.8.7. Effect on blood sugar levels

Locally acting corticosteroids like Dexa promote gluconeogenesis and sugar transport, thus, elevating blood sugar levels [56]. Therefore, the measurement of sugar concentration in the blood is an indirect parameter to assess the enhanced function of Dexa after being released from the nanocargoes in the colon [8]. Both Dexa and Dexa-GP/ES/Pu NCs elevated the sugar content of the blood at the end of the experiment; however, a greater increase was observed with the encapsulated drug inside the nanocargoes (Fig. 6I).

3.8.8. RT-PCR analysis for the expression of regulatory, inflammatory, and mechanistic proteins

iNOS is an inflammatory marker and is elevated in response to free radicals and oxidative species. DSS augmented the expression of colonic iNOS. The iNOS production was significantly diminished by Dexa-GP/ES/Pu NCs treatment ($P < 0.05$) (Fig. 7A1) because of the suppression of inflammatory pathways NF- κ B and COX-2 [57]. Loss of epithelial integrity is a clear manifestation of ulcerative colitis. E-cadherin is one of the tight junction proteins expressed on the intestinal

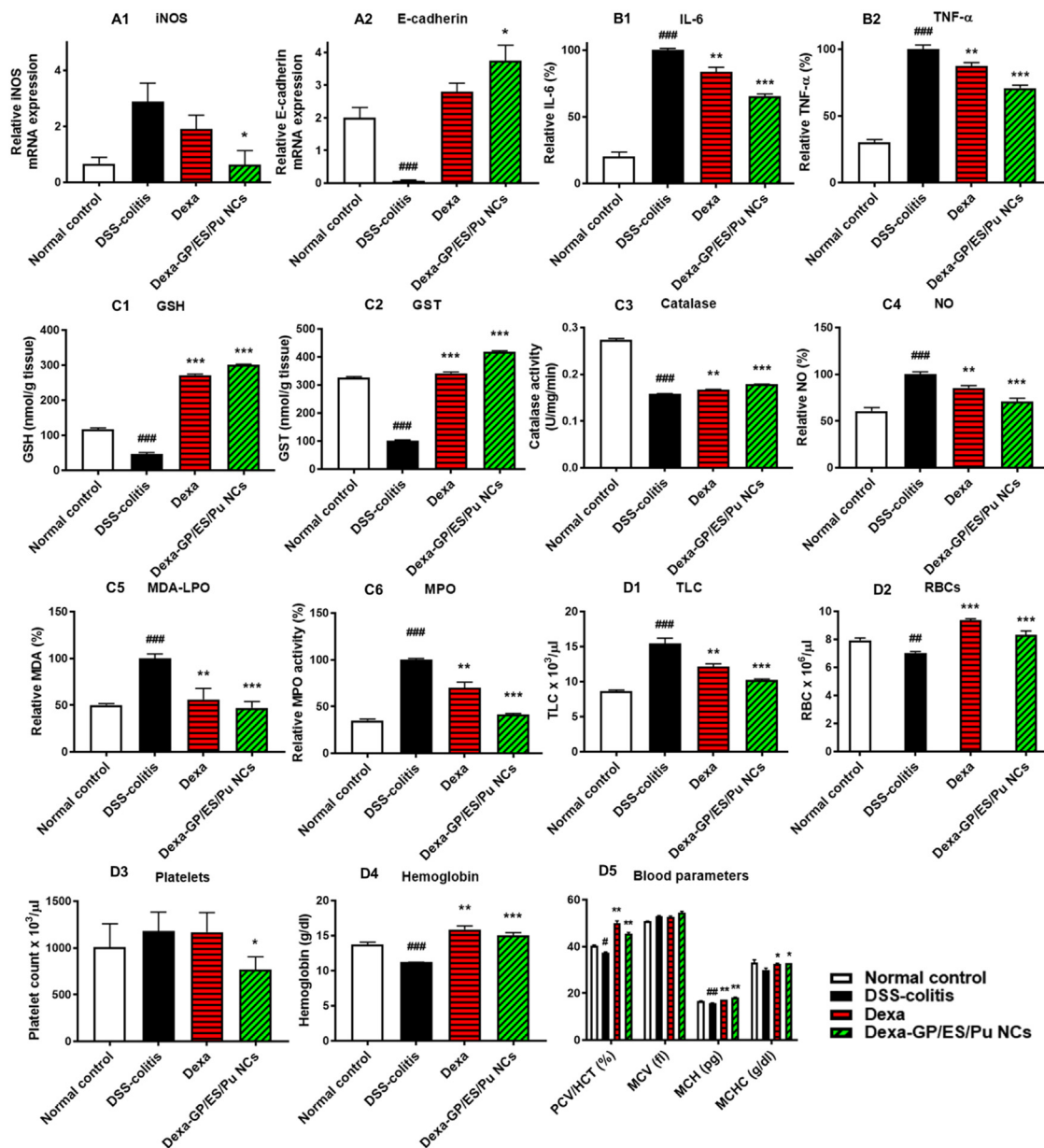


Fig. 7 – Relative mRNA expression of iNOS (a1) and E-cadherin (a2) ($n = 3$) from the colon tissues of different groups under study; Relative percentage of pro-inflammatory cytokines IL-6 (b1) and TNF- α (b2) in the colon tissues of comparative groups ($n = 3$); Concentration of antioxidants GSH (c1), GST (c2), catalase (c3), and oxidants NO (c4), MDA (c5) and MPO (c6) in the excised colon tissues from normal control, DSS-colitis, Dexa and Dexa-GP/ES/Pu NCs treated mice ($n = 3$); Levels of hematological parameters TLC (d1), RBC (d2), Platelets (d3), Hemoglobin (d4), PCV/HCT, MCV, MCH and MCHC (d5) in normal control, DSS-colitis, Dexa and Dexa-GP/ES/Pu NCs treated mice ($n = 3$). Statistical significance between treatment groups and DSS colitis is defined as * $P < 0.05$, ** $P < 0.01$, * $P < 0.001$; the significance levels between Normal control and DSS-colitis are # $P < 0.05$, ## $P < 0.01$, ### $P < 0.001$.**

epithelium; its expression significantly deteriorated in the DSS-induced colitis model (** $P < 0.001$), compared to the normal control. It was found that Dexa-GP/ES/Pu NCs led treatment of the DSS-induced colitis mice resumed the E-cadherins levels up to a marked extent ($P < 0.05$) (Fig. 7A2). Nanocargoes specific delivery of Dexa improved epithelial barrier functions by downregulating pro-inflammatory cytokines, particularly TNF- α [58].

3.8.9. Pro-Inflammatory cytokines detection through ELISA
The levels of IL-6 and TNF- α in the DSS-induced colitis mice considerably diminished with the treatment of both Dexa (** $P < 0.01$) and Dexa-GP/ES/Pu NCs (** $P < 0.001$) (Fig. 7B1-B2). A decrease in IL-6 and TNF- α is directly linked to the downregulation of NF- κ B pathway [59]. Thus, the strategy seems to be effective in neutralizing the pro-inflammatory mediators through the enhanced effect of the drug release

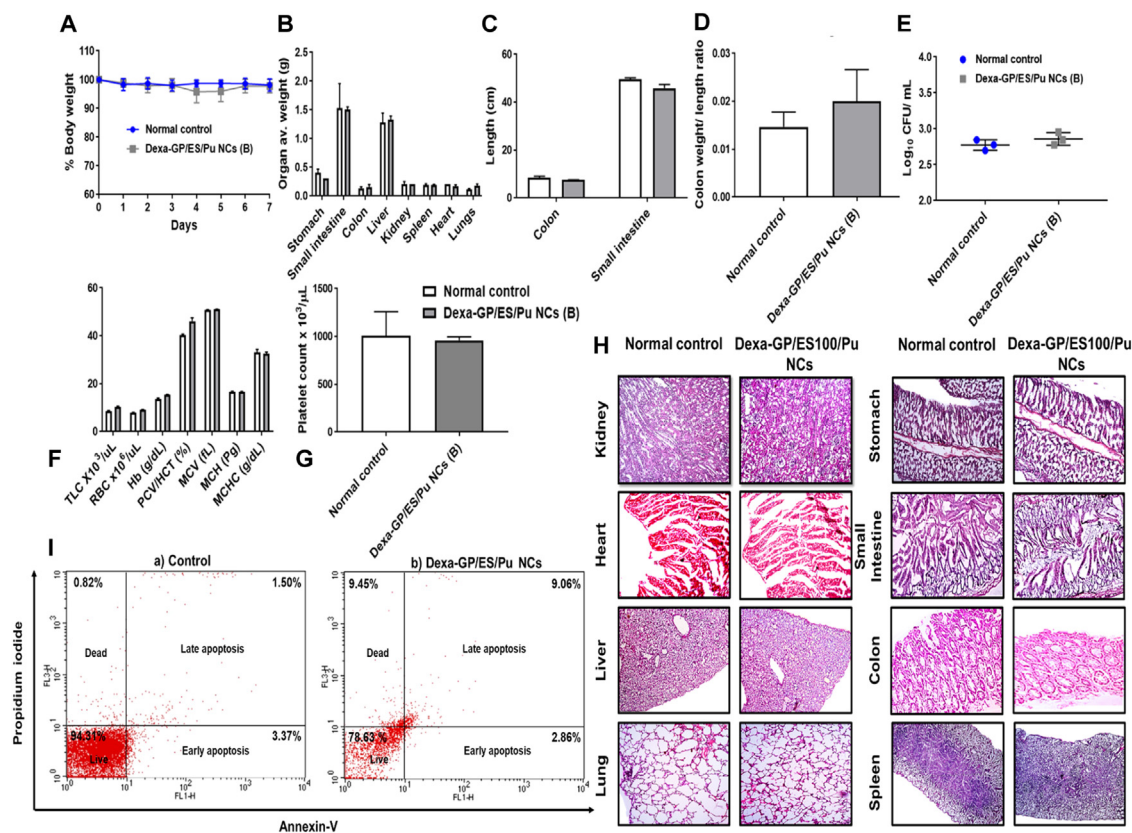


Fig. 8 – Assessment of in-vivo biocompatibility and toxicology during and after 7-d administration of Dexa-GP/ES/Pu to the healthy mice (n = 3): (A) Body weight (%), (B) Average organ weight (g), (C) Intestine lengths (cm), (D) Colon weight to length ratio, (E) Fecal microbial growth (log CFU/ml), (F) Hematological analysis, (G) Platelet count, (H) Histopathological investigations of vital organs (kidney, heart, liver, lung, stomach, small intestine, colon and spleen), (I) Colon cells apoptosis study with Annexin-V/Propidium iodide in the untreated normal healthy control and Dexa-GP/ES/Pu NCs treated healthy mice.

from Dexa-GP/ES/Pu NCs in the inflamed area of the colon.

3.8.10. Biochemical antioxidant assays

Inflammation is proceeded by an oxidative burst and the production of free reactive oxygen species, which in turn overcome the antioxidant scavenging system and damage the cells and barriers. Likewise, DSS elevated the reactive oxygen species and reduced the antioxidant protective enzymes of the intestine ($P < 0.001$ vs normal). Levels of antioxidants including GSH ($P < 0.001$), GST ($P < 0.001$), and catalase ($P < 0.001$) were increased by Dexa-GP/ES/Pu NCs (Fig. 7C1-C3), while oxidative species like NO ($P < 0.001$), and MDA ($P < 0.001$) were significantly reduced by the nanoformulation (Fig. 7C4-C5). Dexa-GP/ES/Pu NCs reduced oxidative stress that diminished NF- κ B activity and thus improved GSH, GST, and catalase levels.

Furthermore, Dexa and Dexa-GP/ES/Pu NCs treatment of DSS induced colitis mice considerably declined MPO activity by 69.7% ($P < 0.01$) and 41.3% ($P < 0.001$) (Fig. 7C6), respectively. In ulcerative colitis, increased immune cell accumulation, especially neutrophils, release MPO enzyme that catalyzes the production of oxidative species to aggravate the inflammation [60]. Therefore, the decline in MPO activity by Dexa-GP/ES/Pu

treatment indicated a decrease in neutrophil activity in the inflamed tissues and thus demonstrated tissue recovery.

3.8.11. Assessment of hematological parameters

Evaluation of the CBC facilitates the diagnosis of the induction and severity of ulcerative colitis and the therapeutic effect of the treatment. DSS-induced colitis raised the levels of TLC to $15.4 \times 10^3 \pm 0.8 \times 10^3$ ($P < 0.001$), compared to the normal values of $8.6 \times 10^3 \pm 0.2 \times 10^3$ (DSS vs normal: $P < 0.001^{###}$). Treatment of colitis with Dexa and Dexa-GP/ES/Pu NCs reduced TLC to $12.13 \times 10^3 \pm 0.42 \times 10^3$ ($P < 0.01^{**}$) and $10.2 \times 10^3 \pm 0.2 \times 10^3$ ($P < 0.001^{***}$), respectively (Fig. 7D1). The RBC levels were decreased by DSS ($P < 0.01^{##}$ vs normal control), which were resumed by both Dexa ($P < 0.001^{**}$) and Dexa-GP/ES/Pu NCs ($P < 0.001^{***}$) treatment (Fig. 7D2). The platelet count was slightly elevated in the DSS colitis group, which was decreased by Dexa-GP/ES/Pu NCs ($P < 0.05^*$ vs DSS) (Fig. 7D3). The other blood parameters including hemoglobin (Hb), packed cell volume/hematocrit (PCV/HCT), mean corpuscular volume (MCV), mean corpuscular hemoglobin (MCH), and mean corpuscular hemoglobin concentration (MCHC) were modified with DSS-induction and successfully normalized with Dexa and Dexa-GP/ES/Pu NCs treatment (Fig. 7D4-D5). Mostly, Dexa-

GP/ES/Pu NCs showed superior efficacy in regulating the blood biochemical values as compared to Dexa only (Fig. 7D1-D5). Blood tests are considered when diagnosing IBD; mostly immune cells are elevated in inflammation, whereas, RBCs are declined in colitis because of anemia. Other blood parameters are also disturbed. Restoration of TLCs, RBCs, hemoglobin levels indicated recovery from DSS-induced inflammation.

3.9. *In vivo* biocompatibility and toxicity investigations of Dexa-GP/ES/Pu NCs

Dexa-GP/ES/Pu NCs were tested in healthy mice to investigate acute toxicity and *in vivo* biocompatibility. During a 7-d course of administration, the mortality rate was negligible with minimal signs of allergy, lethargy, anxiety, and pain. The pattern of food and water intake did not vary. The daily weight assessment (Fig. 8A) showed negligible weight loss in the 7 d ($P=NS$ vs control). After 7 d, mice were euthanized, and major organs were isolated. Organ weight (stomach, small intestine, colon, spleen, liver, kidney, heart and lung), small intestine and colon length, and colon weight-to-length ratio did not differ from the control (Fig. 8B-D). Moreover, feces collected at the end were tested for bacterial count. The total bacterial log CFU/ml was parallel to the control (Fig. 8E), demonstrating that nanocargoes are safe for the natural colon microbiome. In fact, pullulan in the composition of nanoparticles not only improves the colon targeting ability but additionally serves as a probiotic and is beneficial to rectify the colitis-led microbiome disturbances. The biochemical investigation of the blood revealed normal concentrations of RBCs, WBCs and other blood parameters (Fig. 8F and G). Further, the histopathological analysis of the organs had minimal deviations from the control (Fig. 8H). The findings emphasized that Dexa-GP/ES/Pu NCs are nontoxic, biocompatible, and safe in living systems. Further, the apoptotic analysis of colon tissues using Annexin-V and propidium iodide demonstrated that Dexa-GP/ES/Pu NCs exposure resulted in 78.63% live cells as compared to 94.31% live cells in the control (Fig. 8I). The *in vivo* viability percentage mimics the MTT based *in vitro* cell viability range for the colon cells (Fig. 8E-F).

4. Conclusion

Dexa-GP/ES/Pu NCs were fabricated using galactosylated-PLGA polymeric core with encapsulated ES100/Pu coat on the outside of nanocargoes. The nano-formulation was prepared with the desired particle size, zeta potential, PDI, encapsulation efficiency, thermal stability, and FTIR suitability. Nanocargoes retarded drug release at acidic pH with optimal release at colonic pH (7.4) and had good *ex vivo* intestinal retention, *in vitro* macrophage and colon cell uptake, and cellular viability. Nanocargoes had a good colon targeting index inside the UC mice. *In vivo* therapeutic evaluation in the DSS-induced UC model demonstrated excellent tissue restoration and healing processes, manifested through improved morphological parameters, vascular integrity, clinical DAI, histopathological scores, ATR-FTIR analysis, fecal

microbial count, and hematological parameters. Further, NF- κ B and COX-2 downregulation, coupled with decreased iNOS, IL-6 and TNF- α levels, restoration of epithelial integrity, and balancing of antioxidants-oxidants levels reflected enhanced local therapeutic effects. Acute *in vivo* toxicological studies revealed biocompatibility within living system. The current study highlighted the potential of the galactose ligand and ES100/Pu polymeric combination as an inert, nontoxic option to target macrophages in IBD. In short, Dexa-GP/ES/Pu NCs possessed all characteristics to be used as a potential therapy for UC. The prospects include extrapolation of the mechanistic, pharmacokinetic and toxicokinetic aspects of the study and industrial scale-up. Further, large animal tests are required to bring the nanoformulation to human trials.

Declaration of Competing Interest

The authors declared no conflict of interest.

Acknowledgments

I hereby acknowledge the Higher Education Commission of Pakistan for the provision of HEC Indigenous scholarship (PIN No. 315-12214-2BS3-132) for the research work. And for the provision of grant under HEC NRPU project No. 9272/Federal/NRPU/R&D/HEC/2017.

Supplementary materials

Supplementary material associated with this article can be found, in the online version, at doi:10.1016/j.ajps.2023.100831.

REFERENCES

- [1] Tatiya-aphiradee N, Chatuphonprasert W, Jarukamjorn K. Immune response and inflammatory pathway of ulcerative colitis. *J Basic Clin Physiol Pharmacol* 2019;30(1):1-10.
- [2] Mukhtar M, Ali H, Ahmed N, Munir R, Talib S, Khan AS, et al. Drug delivery to macrophages: a review of nano-therapeutics targeted approach for inflammatory disorders and cancer. *Expert Opin Drug Deliv* 2020;17(9):1239-57.
- [3] Zeeshan M, Ali H, Khan S, Khan SA, Weigmann B. Advances in orally-delivered pH-sensitive nanocarrier systems; an optimistic approach for the treatment of inflammatory bowel disease. *Int J Pharm* 2019;558:201-14.
- [4] Chen F, Liu Q, Xiong Y, Xu L. Current strategies and potential prospects of nanomedicine-mediated therapy in inflammatory bowel disease. *Int J Nanomedicine* 2021;16:4225.
- [5] Xu Y, Zhu BW, Li X, Li YF, Ye XM, Hu JN. Glycogen-based pH and redox sensitive nanoparticles with ginsenoside Rh2 for effective treatment of ulcerative colitis. *Biomaterials* 2021;121:1077.
- [6] Jacob EM, Borah A, Pillai SC, Kumar DS. Garcinol encapsulated pH-sensitive biodegradable nanoparticles: a novel therapeutic strategy for the treatment of inflammatory bowel disease. *Polymers* 2021;13(6):862.
- [7] Zeeshan M, Ali H, Khan S, Mukhtar M, Khan MI, Arshad M. Glycyrrhizic acid-loaded pH-sensitive poly-(lactic-co-glycolic

- acid) nanoparticles for the amelioration of inflammatory bowel disease. *Nanomedicine* 2019;14(15):1945–69.
- [8] Ali H, Weigmann B, Neurath M, Collnot E, Windbergs M, Lehr CM. Budesonide loaded nanoparticles with pH-sensitive coating for improved mucosal targeting in mouse models of inflammatory bowel diseases. *J Controlled Release* 2014;183:167–77.
- [9] Qu Z, Wong KY, Moniruzzaman M, Begun J, Santos HA, Hasnain SZ, et al. One-pot synthesis of pH-responsive Eudragit-mesoporous silica nanocomposites enable colonic delivery of glucocorticoids for the treatment of inflammatory bowel disease. *Adv Therapeut* 2021;4(2):2000165.
- [10] Nie Q, Li C, Wang Y, Hu Y, Pu W, Zhang Q, et al. Pathologically triggered *in situ* aggregation of nanoparticles for inflammation-targeting amplification and therapeutic potentiation. *Acta Pharmaceut Sinica B* 2023;13(1):390–409.
- [11] Li C, Zhao Y, Cheng J, Guo J, Zhang Q, Zhang X, et al. A proresolving peptide nanotherapy for site-specific treatment of inflammatory bowel disease by regulating proinflammatory microenvironment and gut microbiota. *Adv Sci* 2019;6(18):1900610.
- [12] Sohail M, Mudassir, Minhas MU, Khan S, Hussain Z, de Matas M, et al. Natural and synthetic polymer-based smart biomaterials for management of ulcerative colitis: a review of recent developments and future prospects. *Drug Deliv Transl Res* 2019;9(2):595–614.
- [13] Luo R, Lin M, Fu C, Zhang J, Chen Q, Zhang C, et al. Calcium pectinate and hyaluronic acid modified lactoferrin nanoparticles loaded rhein with dual-targeting for ulcerative colitis treatment. *Carbohydr Polym* 2021;263:117998.
- [14] Singh RS, Kaur N, Rana V, Kennedy JF. Pullulan: a novel molecule for biomedical applications. *Carbohydr Polym* 2017;171:102–21.
- [15] Singh R, Saini G. Pullulan as therapeutic tool in biomedical applications. *Advances in Industrial Biotechnology India: IK International Publishing House Pvt Ltd*; 2014. p. 263–91.
- [16] Lima IAD, Pomin SP, Cavalcanti OA. Development and characterization of pullulan-polymethacrylate free films as potential material for enteric drug release. *Braz J Pharmaceut Sci* 2017:53.
- [17] de Arce Velasquez A, Ferreira LM, Stangarlin MFL, da Silva CdB, Rolim CMB, Cruz L. Novel Pullulan–Eudragit® S100 blend microparticles for oral delivery of risedronate: formulation, *in vitro* evaluation and tableting of blend microparticles. *Mater Sci Eng: C* 2014;38:212–17.
- [18] Mukhtar M, Zeeshan M, Khan S, Shahnaz G, Khan SA, Sarwar HS, et al. Fabrication and optimization of pH-sensitive mannose-anchored nano-vehicle as a promising approach for macrophage uptake. *Appl Nanosci* 2020;10(11):4013–27.
- [19] Lee Y, Sugihara K, Gilliland MG, Jon S, Kamada N, Moon JJ. Hyaluronic acid–bilirubin nanomedicine for targeted modulation of dysregulated intestinal barrier, microbiome and immune responses in colitis. *Nat Mater* 2020;19(1):118–26.
- [20] Naserifar M, Hosseinzadeh H, Abnous K, Mohammadi M, Taghdisi SM, Ramezani M, et al. Oral delivery of folate-targeted resveratrol-loaded nanoparticles for inflammatory bowel disease therapy in rats. *Life Sci* 2020;262:118555.
- [21] Zeeshan M, Ain QU, Sunny A, Raza F, Mohsin M, Khan S, et al. QbD-based fabrication of transferrin-anchored nanocarriers for targeted drug delivery to macrophages and colon cells for mucosal inflammation healing. *Biomater Sci* 2023.
- [22] Hong L, Kim WS, Lee SM, Kang SK, Choi YJ, Cho CS. Pullulan nanoparticles as probiotics enhance the antibacterial properties of *Lactobacillus plantarum* through the induction of mild stress in probiotics. *Front Microbiol* 2019;10:142.
- [23] Deng F, He S, Cui S, Shi Y, Tan Y, Li Z, et al. A molecular targeted immunotherapeutic strategy for ulcerative colitis via dual-targeting nanoparticles delivering miR-146b to intestinal macrophages. *J Crohn's Colitis* 2019;13(4):482–94.
- [24] Yang M, Zhang Y, Ma Y, Yan X, Gong L, Zhang M, et al. Nanoparticle-based therapeutics of inflammatory bowel diseases: a narrative review of the current state and prospects. *J Bio-X Res* 2020;3(4):157–73.
- [25] Newton R. Molecular mechanisms of glucocorticoid action: what is important? *Thorax* 2000;55(7):603–13.
- [26] Roman-Blas J, Jimenez S. NF- κ B as a potential therapeutic target in osteoarthritis and rheumatoid arthritis. *Osteoarthritis Cartil* 2006;14(9):839–48.
- [27] Zeeshan M, Ali H, Ain QU, Mukhtar M, Gul R, Sarwar A, et al. A holistic QbD approach to design galactose conjugated PLGA polymer and nanoparticles to catch macrophages during intestinal inflammation. *Mater Sci Eng: C* 2021;126:112183.
- [28] Zeeshan M, Atiq A, Ain QU, Ali J, Khan S, Ali H. Evaluating the mucoprotective effects of glycyrrhizic acid-loaded polymeric nanoparticles in a murine model of 5-fluorouracil-induced intestinal mucositis via suppression of inflammatory mediators and oxidative stress. *Inflammopharmacology* 2021;29(5):1539–53.
- [29] Oshi MA, Naeem M, Bae J, Kim J, Lee J, Hasan N, et al. Colon-targeted dexamethasone microcrystals with pH-sensitive chitosan/alginate/Eudragit S multilayers for the treatment of inflammatory bowel disease. *Carbohydr Polym* 2018;198:434–42.
- [30] Yin Y, Chen D, Qiao M, Lu Z, Hu H. Preparation and evaluation of lectin-conjugated PLGA nanoparticles for oral delivery of thymopentin. *J Controlled Release* 2006;116(3):337–45.
- [31] Sohail MF, Javed I, Hussain SZ, Sarwar S, Akhtar S, Nadhman A, et al. Folate grafted thiolated chitosan enveloped nanoliposomes with enhanced oral bioavailability and anticancer activity of docetaxel. *J Mater Chem B* 2016;4(37):6240–8.
- [32] Zhang M, Viennois E, Prasad M, Zhang Y, Wang L, Zhang Z, et al. Edible ginger-derived nanoparticles: a novel therapeutic approach for the prevention and treatment of inflammatory bowel disease and colitis-associated cancer. *Biomaterials* 2016;101:321–40.
- [33] Zhang X, Goncalves R, Mosser DM. The isolation and characterization of murine macrophages. *Curr Protoc Immunol* 2008;83(1) 14.1.1–14.1.14.
- [34] Lu M, Varley AW. Harvest and culture of mouse peritoneal macrophages. *Bio Protoc* 2013;3(22):967–70.
- [35] Gao M, Xu H, Bao X, Zhang C, Guan X, Liu H, et al. Oleonic acid-loaded PLGA-TPGS nanoparticles combined with heparin sodium-loaded PLGA-TPGS nanoparticles for enhancing chemotherapy to liver cancer. *Life Sci* 2016;165:63–74.
- [36] Arifin WN, Zahiruddin WM. Sample size calculation in animal studies using resource equation approach. *The Malaysian journal of medical sciences. MJMS* 2017;24(5):101–5.
- [37] Hubrecht RC, Carter E. The 3Rs and humane experimental technique: implementing change. *Animals* 2019;9(10):754.
- [38] Jerkic M, Peter M, Ardelean D, Fine M, Konerding MA, Letarte M. Dextran sulfate sodium leads to chronic colitis and pathological angiogenesis in Endoglin heterozygous mice. *Inflamm Bowel Dis* 2010;16(11):1859–70.
- [39] Erben U, Lodenkemper C, Doerfel K, Spieckermann S, Haller D, Heimesaat MM, et al. A guide to histomorphological evaluation of intestinal inflammation in mouse models. *Int J Clin Exp Pathol* 2014;7(8):4557.
- [40] Sana E, Zeeshan M, Ain QU, Khan AU, Hussain I, Khan S, et al. Topical delivery of curcumin-loaded transfersomes gel ameliorated rheumatoid arthritis by inhibiting NF- κ β pathway. *Nanomedicine* 2021;16(10):819–37.

- [41] Khan A, Ullah MZ, Afridi R, Rasheed H, Khalid S, Ullah H, et al. Antinociceptive properties of 25-methoxy hispidol A, a triterpenoid isolated from *Poncirus trifoliata* (Rutaceae) through inhibition of NF- κ B signalling in mice. *Phytother Res* 2019;33(2):327–41.
- [42] Baker MJ, Trevisan J, Bassan P, Bhargava R, Butler HJ, Dorling KM, et al. Using Fourier transform IR spectroscopy to analyze biological materials. *Nat Protoc* 2014;9(8):1771–1791.
- [43] Shal B, Khan A, Khan AU, Ullah R, Ali G, Islam SU, et al. Alleviation of memory deficit by bergenin via the regulation of reelin and Nrf-2/NF- κ B pathway in transgenic mouse model. *Int J Mol Sci* 2021;22(12):6603.
- [44] Naeem M, Bae J, Oshi MA, Kim MS, Moon HR, Lee BL, et al. Colon-targeted delivery of cyclosporine A using dual-functional Eudragit[®] FS30D/PLGA nanoparticles ameliorates murine experimental colitis. *Int J Nanomedicine* 2018;13:1225–40.
- [45] Ding D, Kundukad B, Somasundar A, Vijayan S, Khan SA, Doyle PS. Design of mucoadhesive PLGA microparticles for ocular drug delivery. *ACS Appl Bio Mater* 2018;1(3):561–71.
- [46] Chaves PDS, Frank LA, Frank AG, Pohlmann AR, Guterres SS, Beck RCR. Mucoadhesive properties of Eudragit[®] RS100, Eudragit[®] S100, and poly (ϵ -caprolactone) nanocapsules: influence of the vehicle and the mucosal surface. *AAPS PharmSciTech* 2018;19(4):1637–46.
- [47] Vila MMD, Tardelli ER, Chaud MV, Tubino M, Balcão VM. Development of a buccal mucoadhesive film for fast dissolution: mathematical rationale, production and physicochemical characterization. *Drug Deliv* 2014;21(7):530–9.
- [48] Rossi S, Vigani B, Sandri G, Bonferoni MC, Caramella CM, Ferrari F. Recent advances in the mucus-interacting approach for vaginal drug delivery: from mucoadhesive to mucus-penetrating nanoparticles. *Expert Opin Drug Deliv* 2019;16(8):777–81.
- [49] Hua S, Marks E, Schneider JJ, Keely S. Advances in oral nano-delivery systems for colon targeted drug delivery in inflammatory bowel disease: selective targeting to diseased versus healthy tissue. *Nanomed Nanotechnol Biol Med* 2015;11(5):1117–32.
- [50] Yang C, Merlin D. Nanoparticle-mediated drug delivery systems for the treatment of IBD: current perspectives. *Int J Nanomedicine* 2019;14:8875.
- [51] Hwang YJ, Nam SJ, Chun W, Kim SI, Park SC, Kang CD, et al. Anti-inflammatory effects of apocynin on dextran sulfate sodium-induced mouse colitis model. *PLoS One* 2019;14(5):e0217642.
- [52] Andronie L, Cîntă Pânzaru S, Cozar O, Domşa I. FT-IR spectroscopy for human colon tissue diagnostic. *Rom J Biophys* 2011;21(2):85–91.
- [53] Li Q, Hao C, Kang X, Zhang J, Sun X, Wang W, et al. Colorectal cancer and colitis diagnosis using Fourier transform infrared spectroscopy and an improved K-nearest-neighbour classifier. *Sensors* 2017;17(12):2739.
- [54] Bangaoil R, Santillan A, Angeles LM, Abanilla L, Lim A Jr, Ramos MC, et al. ATR-FTIR spectroscopy as adjunct method to the microscopic examination of hematoxylin and eosin-stained tissues in diagnosing lung cancer. *PLoS One* 2020;15(5):e0233626.
- [55] Khan I, Ullah N, Zha L, Bai Y, Khan A, Zhao T, et al. Alteration of gut microbiota in inflammatory bowel disease (IBD): cause or consequence? IBD treatment targeting the gut microbiome. *Pathogens* 2019;8(3):126.
- [56] Thiesen A, Wild G, Tappenden K, Drozdowski L, Keelan M, Thomson B, et al. The locally acting glucocorticosteroid budesonide enhances intestinal sugar uptake following intestinal resection in rats. *Gut* 2003;52(2):252–9.
- [57] Al-Harbi NO, Imam F, Al-Harbi MM, Ansari MA, Zoheir KM, Korashy HM, et al. Dexamethasone attenuates LPS-induced acute lung injury through inhibition of NF- κ B, COX-2, and pro-inflammatory mediators. *Immunol Invest* 2016;45(4):349–69.
- [58] Boivin MA, Ye D, Kennedy JC, Al-Sadi R, Shepela C, Ma TY. Mechanism of glucocorticoid regulation of the intestinal tight junction barrier. *Am J Physiol-Gastrointestinal Liver Physiol* 2007;292(2):G590–G598.
- [59] Liu T, Zhang L, Joo D, Sun SC. NF- κ B signaling in inflammation. *Signal Transduct Targeted Therapy* 2017;2(1):17023.
- [60] Chami B, Martin NJ, Dennis JM, Witting PK. Myeloperoxidase in the inflamed colon: a novel target for treating inflammatory bowel disease. *Arch Biochem Biophys* 2018;645:61–71.